To the Graduate Council:

I am submitting herewith a thesis written by Jack Leland Parker entitled "Evaluation of a Submicron Particulate Monitor." I have examined the final copy of this thesis for form and content and recommend that it be accepted in partial fulfillment of the requirements for the degree of Master of Science, with a major in Physics.

A. A. Mason, Major Professor

We have read this thesis and recommend its acceptance:

Accepted for the Council:

Associate Vice Chancellor
and Dean of the Graduate School

STATEMENT OF PERMISSION TO USE

In presenting this thesis in partial fulfillment of the requirements for a Master's degree at The University of Tennessee, Knoxville, I agree that the Library shall make it available to borrowers under rules of the Library. Brief quotations from this thesis are allowable without special permission, provided that accurate acknowledgment of the source is made.

Permission for extensive quotation from or reproduction of this thesis may be granted by my major professor, or in his absence, by the Head of Interlibrary Services when, in the opinion of either, the proposed use of the material is for scholarly purposes. Any copying or use of the material in this thesis for financial gain shall not be allowed without my written permission.

Signature Jack Harker

Date 3 December 1993

EVALUATION OF A SUBMICRON PARTICULATE MONITOR

A Thesis

Presented for the Master of Science

Degree

The University of Tennessee, Knoxville

Jack Leland Parker

December 1993

ACKNOWLEDGMENTS

First I thank my immediate work supervisor, Dr. Thomas V. Giel, Jr., for the guidance he gave while I was carrying out the work presented in this thesis. I also thank him for his help in preparing the thesis itself. I also appreciate all of the other members of my committee, Dr. Arthur A. Mason, Dr. Horace Crater, Dr. Christian Parigger, and Dr. Bradley C. Winkleman, for their suggestions and comments on the presentation of this work. I am grateful for the personnel at the Department of Energy CFFF and particularly for those in the particulate sampling group. Without their assistance I could not have completed this work. Bill Millard was especially helpful in all of the supporting experiments I had to do. Jeff Holt and Mike Hodges were very helpful when I had questions about the theory and operation of the system.

I also thank Mark Meadors of Particle Measuring Systems, Inc., for his hard work in helping me overcome the problems encountered with the particle sizing devices. I acknowledge Particle Measuring Systems, Inc. and McGraw Hill Book Company for their permission in using figures from their publications.

I acknowledge the Department of Energy and the State of Tennessee who supported me financially while I was at the University.

I thank my family and especially my wife Collette for their support during the time I worked on this thesis.

ABSTRACT

A Sample Extraction / Dilution System (SEDS) was built at The University of Tennessee Space Institute (UTSI) to measure particle size distributions and mass loadings in a high number density environment. The SEDS extracts a sample of particle laden gas from a high particle concentration environment and dilutes it while preventing acid and water condensation. After dilution, a commercially available particle sizing instrument can be used for number density and mass loading measurements. The major advantage of the SEDS over currently available techniques for measuring high loading environments is its on-line, near real-time response to particle number density fluctuations.

The performance limitations and uncertainties of the SEDS is evaluated, both theoretically and experimentally. The theoretical evaluation is done with supporting experiments by considering each contributing element to the measurement individually. By propagating the errors through a Taylor series expansion, the largest contributing factor to the overall uncertainty can be identified. From this investigation, the largest error source was the unsteady sample flow of the commercial particle sizing instruments. The uncertainty limit is estimated to be ±32%. When the error due to the varying flow rates is removed, the uncertainty limit reduces to ±20%.

Experiments were carried out at the U. S. Department of Energy Coal Fired Flow Facility (CFFF) adjacent to UTSI to evaluate directly the SEDS performance. The purpose of these tests was to compare measurements made with the SEDS to those made with an accepted standard particle sampling method (5 stage cyclone). However, during the tests, the sample orifice and the tubing within the SEDS plugged gradually. This shut off the flow of particles. When a larger orifice was installed to prevent plugging, the particle counters became saturated. The SEDS also had difficulty in drawing a

representative sample from the flue duct. The pressure inside the flue at the CFFF stays at about 8% below atmospheric pressure. The pumps on the SEDS could not adequately sample the gas from this low pressure region. Because of these difficulties, no direct comparison could be made between the SEDS and the 5 stage cyclone.

To evaluate fully the SEDS, the plugging needs to be eliminated by redesigning the extraction system. This should promote better sampling from the duct. Also, by modifying the individual components of the SEDS and the particle sizing instruments, the accuracy of the system will be improved.

TABLE OF CONTENTS

CHAPTER		PAGE
I.	Introduction	1
	Particles and Particulate Measuring	1
	Particulate Production in MHD	1
II.	Background	4
	MHD Power Generation	4
	Advantages	5
	Disadvantages	5
	Health Concerns over Airborne Particulate	8
	Emissions Monitoring	8
	SEDS	11
	Purpose of Thesis	11
III.	System Description	13
	SEDS	13
	PMS ASASP-X -- Theory of Operation	15
	PMS ASASP-X -- Air Flow	16
	PMS ASASP-X -- Optical System	19
	Advantages of the PMS ASASP-X	21
	Aerodynamic vs. Optical Measuring	23
	Data Acquisition and Analysis	23
IV.	Determination of Uncertainties	25
	Nature of Error and Uncertainty	25
	5 Stage Cyclone	25

Insitec, Inc.....27
SEDS Uncertainty -- Experimental.....29
SEDS Uncertainty -- Theoretical.....32
Evaluation of Uncertainty Due to Individual Components.....34
Time Interval.....34
Sample Flow Rate.....34
Correction Factor.....36
Event Counts.....40
Dilution Ratio.....43
V. Uncertainty Results.....47
Overall Uncertainty: vs. 5 Stage Cyclone.....47
Component Uncertainty.....55
Time Interval.....56
Sample Flow Rate.....56
Correction Factor.....59
Event Counting.....62
Dilution Ratio.....71
Total Theoretical Uncertainty Limit.....71
VI. Conclusions and Recommendations.....75
List of References.....77
Appendices.....80
Appendix A. Commercially Available Particulate Sizing Instruments
Considered for the SEDS.....81
Bausch and Lomb.....81
Climet Series 7000.....81
Dynac.....81

Gardner.....82

Techecology.....82

Appendix B. Calculation of Orifice Calibration Parameters K and b and their Respective Uncertainties.....83

Vita.....88

LIST OF TABLES

TABLE		PAGE
1	Particle Size Ranges for Bins of the PMS ASASP-X	22
2.	Bin Sizes of the 5 Stage Cyclone	28
3.	Results of Calibration Check for Sample Flow Meters	58
4.	Results of Measurements to Find *M* and its Uncertainties	67
5.	Summary of Measurements to Find *M* and its Uncertainties	69
6.	Results of Measurements to Find *Z* and its Uncertainties	72
7.	Final Uncertainty Analysis for SEDS	74
B1.	Data Points for Calibration Constant Calculation	84
B2.	Results of Uncertainty Analysis for Orifice Calibration Constants	87

LIST OF FIGURES

FIGURE		PAGE
1.	Typical Particle Size Loading at BH/ESP Inlet	6
2.	Particle Removal Efficiencies for Typical BH and ESP Collection Devices	7
3.	Temporal Fluctuations in Particle Volume Concentration	10
4.	Schematic Diagram of the Sample Extraction/Dilution System (SEDS)	14
5.	Calculated Mie Scattering Curves for the PMS ASASP-X	17
6.	Airflow System of the PMS ASASP-X	18
7.	Optical System of the PMS ASASP-X	20
8.	Concept of Error and Uncertainty	26
9.	Schematic Diagram of Calibration Rig Used for Simultaneous Experiments with Insitec, Inc	30
10.	Schematic Diagram of Sample Duct Used for Collection of Fluidized Ash Particles	39
11.	Schematic Diagram of Nebulizer System	41
12.	Schematic Diagram of Drying Chamber Used with Nebulizer System	42
13.	Typical Data Collected by the 5 Stage Cyclone at the BH/ESP Inlet	48
14.	Total Number Density as Measured Through the SEDS Decreasing with Time	49
15.	Correspondence of Particle Concentration Distribution and Activity of Particle Spectrometer with Time	50
16.	Schematic Diagram of Sample Orifice in SEDS	51
17.	Relative Pressure Changes Due to Flow Through an Orifice	52

18. Calibration Comparison of SEDS and Insitec PCSV-UFP.....54

19. Divergence in Agreement Between Two Particle Spectrometers.....60

20. Measurements made with Monodisperse Particles to Verify Accuracy in Response of ASASP-X.....63

LIST OF ABBREVIATIONS

ASASP-X ..... Active Scattering Aerosol Spectrometer Probe

BH ..... Baghouse

CFFF ..... Coal Fired Flow Facility

DESP ..... Dry Electrostatic Precipitator

DOE ..... Department of Energy

EPA ..... Environmental Protection Agency

ESP ..... Electrostatic Precipitator

MHD ..... Magnetohydrodynamics

MSU ..... Mississippi State University

NO_x ..... Nitric Oxides

PCSV ..... Particle Counter, Sizer, Velocimeter

PMS ..... Particle Measuring System

PSL ..... Polystyrene Latex

SO_x ..... Sulfur Oxides

SEDS ..... Sample Extraction Dilution System

UTSI ..... University of Tennessee Space Institute

UFP ..... Ultra Fine Probe

WESP ..... Wet Electrostatic Precipitator

LIST OF SYMBOLS

b ..... Calibration Parameter for Best Data Fit

B ..... Bias

BP ..... Barometric Pressure

D ..... Particle Diameter

dN/dD ..... Number Density Normalized with Bin Width

$dN/dlogD$ ..... Number Density Normalized with Logarithmic Bin Width

f ..... Mass Fraction of Water in a Gas Sample

IC ..... Influence Coefficient

K ..... Orifice Calibration Constant

m ..... Mass

M ..... Events Counted by the PMS ASASP-X

mw ..... Molecular Weight

N ..... Calculated Number Density

P ..... Absolute Pressure

P' ..... Static Pressure

ΔP ..... Pressure Drop

q ..... True Value of Quantities

Q ..... Mass Flow Rate

R ..... Sample Flow Rate of the ASASP-X

S ..... Random Error

T_R ..... Absolute Temperature (Rankine scale)

T_F ..... Relative Temperature (Fahrenheit scale)

t ..... Time Interval

U ..... Uncertainty Limit

x ..... Measured Quantities

Z ..... Dilution Ratio

α ..... Correction Factor

β ..... Bias from One Elemental Source

Δ ..... Difference in Measured Number Densities

ε ..... Efficiency of Ideal Heat Engine

σ ..... Standard Deviation of One Elemental Source

L ..... Subscript; Denotes Large Air Orifice

S ..... Subscript; Denotes Small Air Orifice

CHAPTER I
Introduction

Particles and Particulate Measuring

Particle measuring technology involves a variety of methods and applications. The technology has developed rapidly in the past few years being driven by the need for devices with improved resolution and reliability. Environmentally speaking, particle measurement is essential. Legislation requires that manufacturers carefully monitor and control their particulate emissions. In places like quarries, mines, and factories, the airborne particulate concentration can be very heavy. In many states and cities, automobile emissions are monitored in an effort to curb the increase of atmospheric pollution. Nature also contributes atmospheric particulate content through volcanoes, forest fires, and wind storms. These airborne particulates pose a potential health hazard.

Particulate Production in MHD

The Coal Fired Flow Facility (CFFF) has been operated by The University of Tennessee Space Institute (UTSI) for the U. S. Department of Energy to study the proof of concept of coal fired magnetohydrodynamics (MHD). A coal fired MHD process used as the topping cycle to a standard fossil fuel power plant should provide improved electrical power plant efficiency and decreased toxic gas emissions. However, the coal fired MHD process produces a large number of submicron particles in the exhaust flue gas. For coal fired MHD to be environmentally acceptable, a suitable flue gas particulate removal system is necessary. An accompanying monitoring device is required to determine the efficiency of the particulate cleanup systems. At the CFFF, research has been conducted to improve

particle removal systems. The systems used are a Baghouse (BH), a Wet Electrostatic Precipitator (WESP), and a Dry Electrostatic Precipitator (DESP).

To improve the particulate removal efficiency of the BH, WESP, and DESP, it is necessary to monitor the particle concentration both upstream and downstream of these devices. By changing operating conditions and noting how the changes affect particulate removal, it is possible to optimize the particle removal efficiency. The monitoring of this process must be done with near real-time capability. No instrumentation is currently available that can monitor in real time the high particle loading found at the CFFF. For this purpose, UTSI built a Sample Extraction / Dilution System (SEDS) that extracts and dilutes a sample of flue gas allowing real-time, on-line analysis with commercially available instrumentation. The purpose of this thesis is to determine the performance limitations and measurement uncertainties of the SEDS. Experimentally, the SEDS can be evaluated by comparing measurements taken with the SEDS to measurements taken with other particulate monitoring devices. Theoretically, uncertainties can be calculated for each of the contributing components. By doing this, the largest contributing factors to measurement uncertainties can be addressed. Both of these approaches are taken in this thesis.

Chapter II of this thesis will give a brief background of power generation by coal fired MHD. Discussed in this chapter will be some of the advantages and disadvantages of the MHD process, including the health concern over submicron particles. The current emissions control and monitoring used and being tested at the CFFF, including the SEDS will also be discussed.

Chapter III describes the SEDS, discussing in detail the instruments used to extract the sample from the flue duct and to measure the density of particles. Also described is the data acquisition and analysis configuration. A discussion of the differences between the current standard particulate monitoring methods used and the method being developed is included.

Chapter IV is the theory section wherein the nature of error and uncertainty is addressed. This is followed by an evaluation of the uncertainties of the system and each of its components. The accuracy of the measurements taken by the SEDS versus those taken by a 5 stage cyclone and a probe being developed by Insitec, Inc is determined.

Chapter V contains the numerical results of the study based on the theory of chapter IV. A discussion of problems encountered and suggested solutions are included.

Chapter VI contains the summary and recommendations for future work.

CHAPTER II
Background

MHD Power Generation

Electric power generation through the MHD process relies on the interaction of moving charges with electromagnetic fields. An ionized gas flow through a magnetic field induces an electric field. This electric field generates a direct current through electrodes placed in the MHD channel walls. The direct current from the electrodes is inverted to 60 hertz alternating current. Heat energy in the MHD topping cycle exhaust is extracted in a bottoming cycle and converted to electrical energy via conventional steam turbine power plant technology.

MHD generators operate at higher temperatures than conventional fossil fuel power plants, thereby increasing the overall possible efficiency. This follows from the efficiency equation of an ideal heat engine:

$$\varepsilon = 1 - \frac{T_{cold}}{T_{hot}}, \tag{1}$$

where T is measured on the Kelvin scale. The increased efficiency of the combined MHD and steam cycles reduces the environmental impact of exhaust gases per kilowatt of electrical power generated.

Coal fired MHD operates at high combustion temperatures (typically 3000K). Pulverized coal is used to increase combustion rates. As a consequence, heat loss is reduced. A pressure of up to 10 atmospheres in the combustor forces the hot gas through the generator. Seed in the form of potassium carbonate (K_2CO_3) or potassium formate ($KCHO_2$) is added to provide a medium that easily ionizes thermally at temperatures and

pressures typical for coal fired MHD. The ionized seed generates the necessary conducting fluid.

Advantages

One advantage of the MHD process results from higher, more efficient combustion temperatures. Since carbon conversion is greater, atmospheric emissions of carbon dioxide per electrical kilowatt are reduced. A second advantage is the staged combustion at the CFFF, which has been shown to control the output of NO_x to well below the Environmental Protection Agency (EPA) guidelines. A third advantage is that reduced SO_x concentrations occur in the flue gas due to chemical reactions of the potassium with the sulfur.

Disadvantages

The major disadvantage of coal fired MHD is the increase in the number density of very small particles due to the increased combustion temperature and its effect on particle formation. During MHD combustion most of the species is vaporized or liquefied. The gases condense and nucleate into very small particles as the exhaust cools. The CFFF uses an impact wall at the entrance of the bottoming cycle to remove the large slag particles and droplets. Most of the ash particles that are found past the impact wall are formed by condensation and nucleation. These resulting particles are smaller than fly ash from a typical coal combustion power plant [1]. Figure 1 shows the results of measurements taken at the CFFF using a 5 stage cyclone. The submicron particle loading is on the order of 10^8 particles per cc., posing a health concern of particulate emissions of submicron particles. Figure 2 shows that particles with diameters greater than 0.1 micron and less than 1.0 micron are most difficult to capture with standard control devices such as the BH and electrostatic precipitators (ESP). The particle penetration is the percentage of particles not captured.

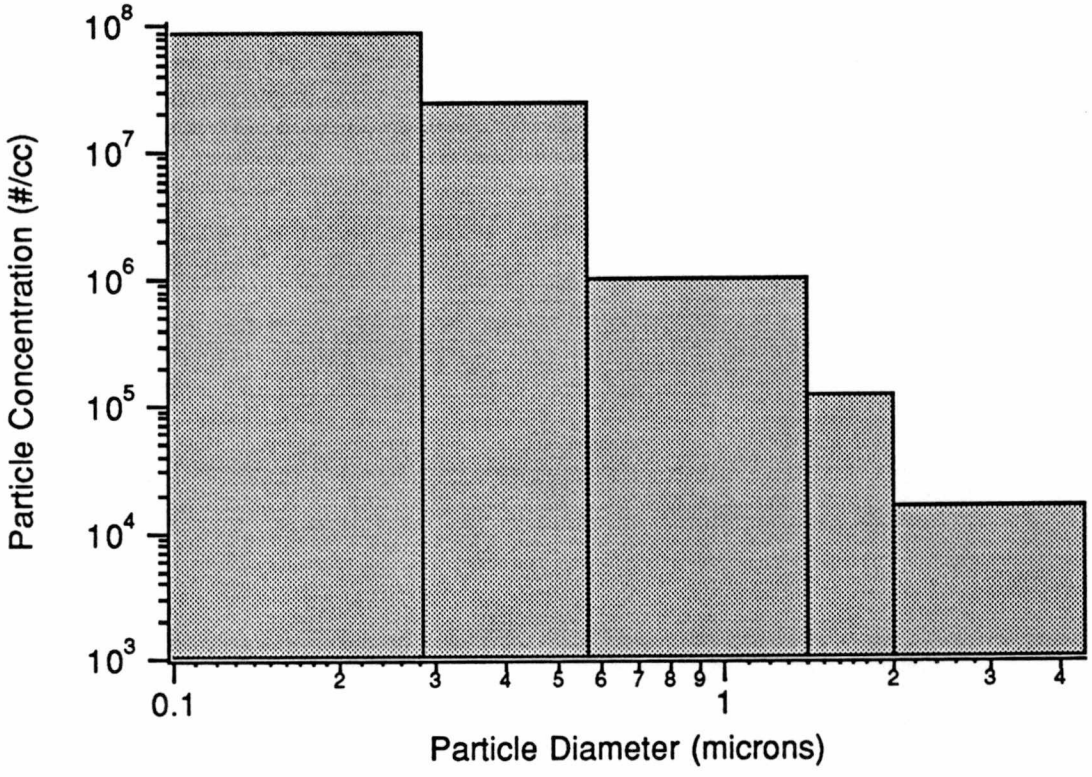


Figure 1. Typical Particle Size Loading at BH/ESP Inlet.

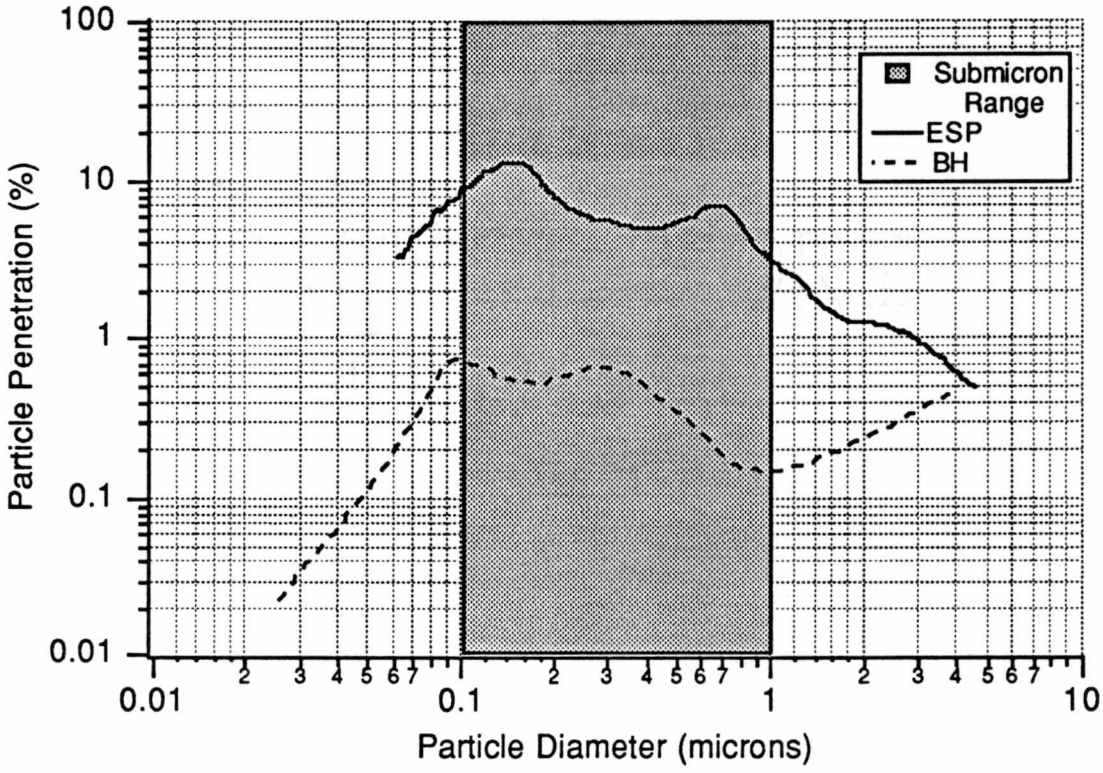


Figure 2. Particle Removal Efficiencies for Typical BH and ESP Collection Devices [3].

Health Concerns over Airborne Particulate

Airborne particulates pose a potential health hazard [1]. Human adult lungs have a volume of typically 5500 cm^3, of which only about half are filled with air constantly being inhaled and exhaled, even during physical activity [2]. The transport of oxygen, carbon dioxide, and particles to the lung tissue is a diffusion process. Particles of diameter less than about 0.1 microns diffuse very slowly. Most are exhaled before they have the chance to penetrate the ambient layer of air. Particles of larger than about 1.0 microns more easily pass through this layer, but are captured by the cilia that line the lungs. The cilia transport the particles back toward the mouth and nose where they are expectorated. Particles in the size range between 0.1 and 1.0 micron are likely to penetrate to the lung tissue but are not likely to be captured by the cilia. When trapped in the lung tissue, the particles can cause a variety of health problems.

Emissions Monitoring

Current accepted standards of emissions monitoring include the method 17 mass loading for total mass emissions and the 5 stage cyclone for size distributions. The method 17 mass loading samples the gas isokinetically from the flue. The velocity of the gas stream is measured, and subsequently a volume that would move at that rate is pumped from the stream over a specified time period. The sampled gas runs through a filter for the purpose of collecting the particles. The filter is weighed and the total mass loading is calculated.

The 5 stage cyclone also samples isokinetically. However, the particle stream goes through a series of cyclones of different sizes. In the cyclones, particles with a linear momentum above a certain threshold impact the walls of the cyclone, and therefore, are removed from the sample. The rest of the particles swirl around to the next stage. The final stage is a calibrated absolute filter. As with the method 17, the total mass of the

particles collected in each stage is measured. From the sample rate, nominal size, and mass of the particles in each bin, the size distribution is inferred.

Although the method 17 and 5 stage cyclone are accepted as standard methods, they are very labor intensive, involving one half to twelve hours of sampling and two to seven days of preparation and measurement evaluation. They offer no real-time or on-line analysis--they cannot monitor changes in plant operation conditions or fuel chemistry. The 5 stage cyclone also yields a poor size resolution. It cannot detect temporal fluctuations of the particle concentration that are known to occur [4]. Figure 3 illustrates such temporal fluctuations at the CFFF, measured by applying optical techniques [5].

To improve the effectiveness of the BH, DESP, and WESP in removing submicron particulates, modifications to these devices and appropriate control of operating conditions are needed. To evaluate the effectiveness of these modifications and different operating conditions, measurements are made both upstream and downstream from the particulate control devices and the results are compared. On-line, real-time analysis is necessary to monitor the fluctuations and their effect on particle removal.

The U. S. Department of Energy has funded efforts to develop devices to monitor the high loading, high temperature conditions found at the CFFF. Mississippi State University (MSU) developed a two color laser transmissometer and an optical size distribution monitor [4]. Insitec, Inc. developed a Particle Counter, Sizer, Velocimiter-Ultra Fine Probe (PCSV-UFP) to measure the volume concentration and the size distribution [5]. Although these instruments permit near real-time analysis, none is yet adequate for the high temperature, high concentration conditions found at the BH/ESP inlet at the CFFF. MSU's instruments can measure particle sizes only down to about 5 microns in diameter and a mass loading only for particles of greater than about 0.8 microns in diameter. Insitec's particle size distribution probe can measure down to about 0.2 microns in low number density environments, but in the high number density environments like those found in the flue just before the particle removal systems, the limit is about 0.8

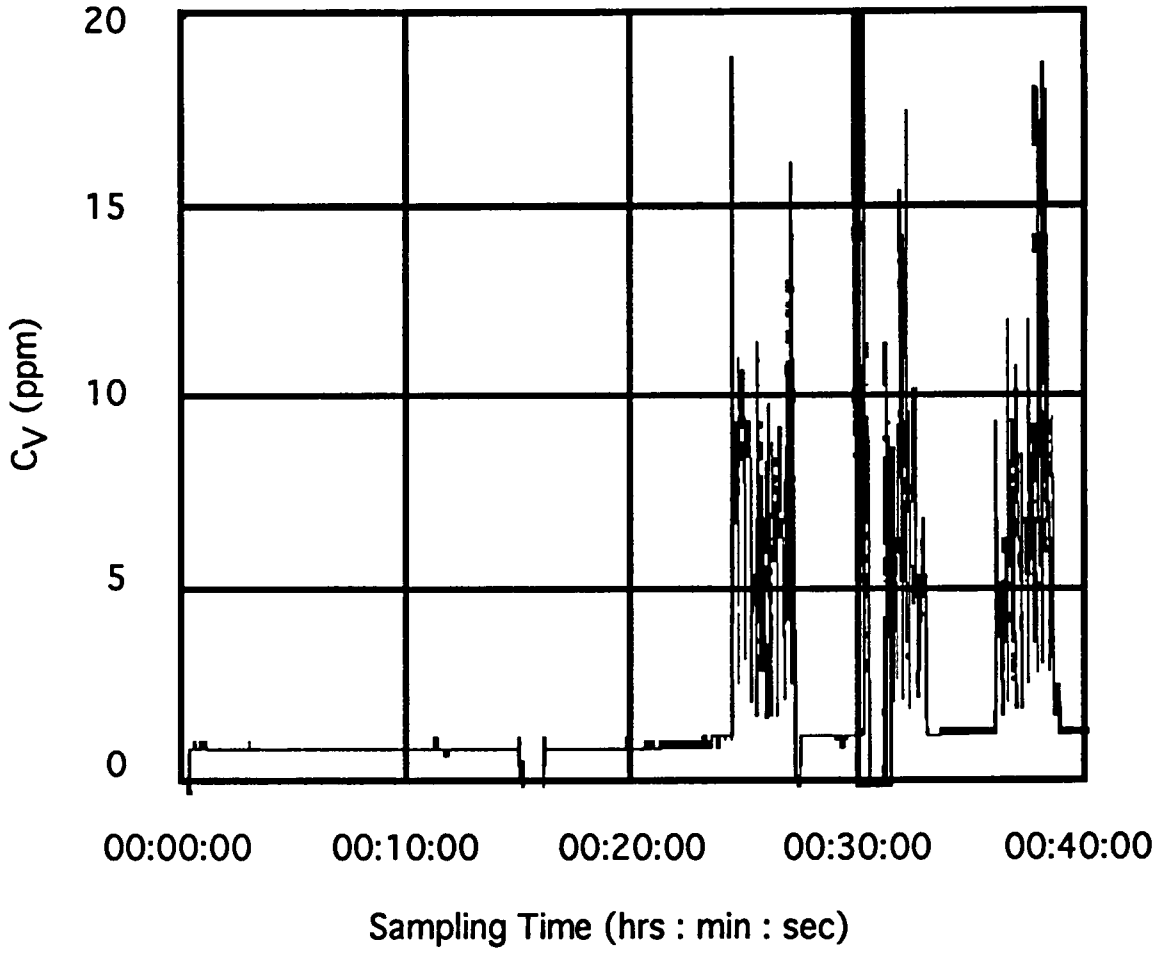


Figure 3. Temporal Fluctuations in Particle Volume Concentration.

microns. Furthermore, measurement uncertainties associated with these instruments are yet to be determined. Other commercially available instruments investigated have similar limitations (see Appendix A). Because of the high mass loading found in MHD combustion exhaust, a dilution system was necessary to make particle size distribution and particle loading measurements.

SEDS

In order to develop a suitable particulate monitoring device for the CFFF conditions, the particulate monitoring group at UTSI built a Sample Extraction / Dilution System (SEDS) modeled after a system developed by Southern Research Institute [6]. The SEDS extracts a sample of gas from a high particle concentration environment and dilutes it without acid or water condensation. The SEDS allows for near real-time, on-line analysis of a sample with a commercially available instrument. The SEDS used at the CFFF was designed to monitor the particulate loading as a function of potassium content, K_2/S ratio, coal flow, coal ash content, stoichiometry, and other appropriate variables. UTSI purchased two particle spectrometers [7] to use with the SEDS. The instruments were purchased in anticipation of simultaneous use upstream with the SEDS and downstream from the particle removal devices. This arrangement allows for near real-time analysis of the effectiveness of the BH and the ESP particulate removal provided that the SEDS performs well.

Purpose of Thesis

The purpose of this thesis is to investigate the performance of the SEDS, defining appropriate operating parameters and the related uncertainties associated with a measurement using the SEDS. A direct way of evaluating the performance and uncertainties of the SEDS is to compare the measurements obtained from the SEDS with

those from the 5 stage cyclone. The 5 stage cyclone is used for the comparison because it is accepted by the EPA as a standard method for particle size distribution measurements.

To improve the performance and to minimize the uncertainties, an investigation of the individual uncertainties that contribute to the system uncertainty is needed. These uncertainties comprise the SEDS pressure, temperature, and orifice calibration uncertainties, and the particle measuring instruments flow rate and calibration uncertainties. By knowing how each component contributes to the overall uncertainty, steps can be taken to systematically minimize significant component uncertainties and thus minimize the measurement uncertainty of the system.

CHAPTER III
System Description

SEDS

In the Sample Extraction / Dilution System (SEDS) a sample of flue gas is extracted and diluted sufficiently at a variable dilution ratio to allow for particle size distribution and mass loading measurements. The extracted sample is maintained at flue temperature until it is diluted with clean, cool, dry gas to prevent any acid or water condensation that would affect the measurement of particle sizes. Variable dilution enables the use of a commercially available on-line particle counter. The SEDS used at Southern Research Institute employs an electrical aerosol analyzer to measure size distributions in the 0.01 to 0.2 micron range; this is an order of magnitude below the region of interest at the CFFF. Although the SEDS was designed for particulate monitoring of particles below 0.5 microns, Southern Research Institute tested the device for particles with diameters of up to 2.3 microns with satisfactory results [6, pages 127-141].

Figure 4 shows a schematic of the SEDS. A sample of particle laden gas is removed from the flue through a heated probe and directed into an oven. The heated probe and oven maintain the sample temperature above the dew point of acid mist and water vapor, which are dependent on gas temperature, pressure, and concentration. If acid or water condenses, large numbers of small droplets form and a condensate covers the particles resulting in biased particle sizes. In the oven, the gas flow is split with most of the sample drawn through the sample pump. A small amount of the gas is drawn through a cyclone designed to remove particles greater than 2.0 microns in diameter. Particles larger than this size are easily removed by the BH and ESPs, and therefore are of no great importance to MHD environmental impact. Also, larger particles may plug the metering

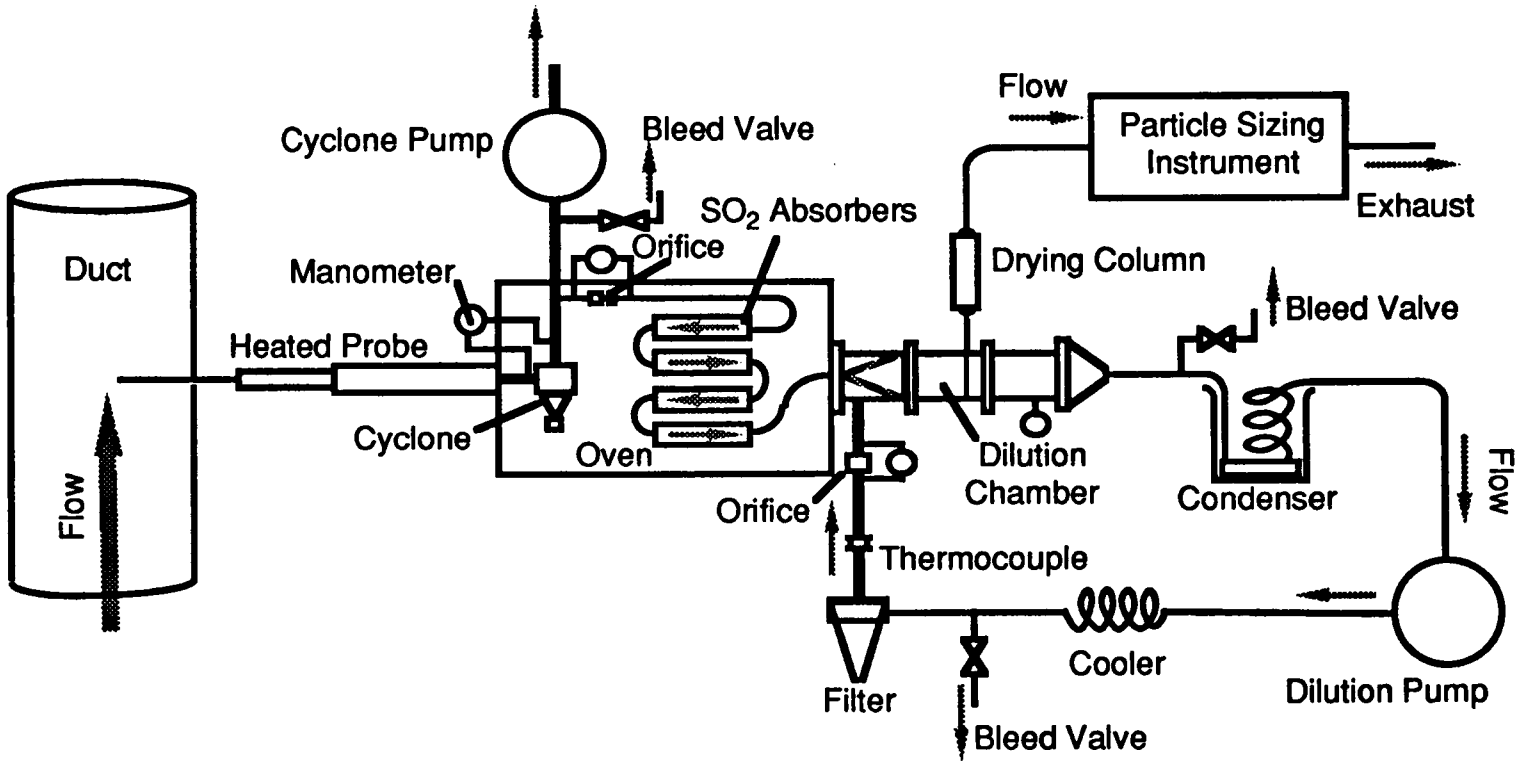


Figure 4. Schematic Diagram of the Sample Extraction / Dilution System (SEDS).

orifice and/or settle in tubing within the SEDS and thus are removed to improve SEDS operation. After the cyclone, the sample passes through the sample metering orifice and a battery of activated charcoal gas diffusion tubes to remove SO_x from the sample.

The sample then passes through the apex of a perforated cone which contains two strips of polonium-210 to neutralize particle charge. Clean, cool, dry flue gas drawn at a metered rate through the perforations of the cone creates a highly turbulent mixing zone in the dilution chamber. Downstream of the mixing zone, a sample is withdrawn by a particle sizing instrument. The remaining flue gas flows through the dilution pump, a cooler to condense the water vapor and a 0.02 micron filter to remove detectable particles. The gas then returns to the dilution chamber through a metering orifice as clean, dry mixing gas. The internal flow system of the SEDS uses, clean, dry flue gas rather than air as the dilution gas. This prevents the possibility of unwanted chemical reactions in the dilution chamber.

To adjust the dilution of the SEDS, all static pressures of the orifice inlets, pressure drops across the orifices, and the temperature of the gas entering the orifice are monitored. All pressures are measured with Magnehelic pressure transducers and all temperatures are measured with type K thermocouples. Uncertainties in these dilution rates will contribute to uncertainties of measurements with the SEDS.

PMS ASASP-X -- Theory of Operation

The particle counter used with the SEDS at the CFFF is the Particle Measuring System's (PMS) Active Scattering Aerosol Spectrometer Probe (ASASP-X) [7]. The instrument is a single particle counter that operates on the theory of Mie scattering. Mie theory predicts that the intensity of the light that is scattered from a plane wave by a particle is a function of the wavelength of the incident radiation, the particle's size, and the particle's index of refraction, assuming spherical particles [8, 9, 10, 11, 12]. Although there is a dependence on particle index of refraction, theoretical Mie curves calculated for

the PMS instrument show that the intensity of scattered radiation versus particle diameter is nearly the same for the particles prevalent at the CFFF, and for polystyrene latex (PSL) calibration particles. The different indices of refraction do not significantly affect the ASASP-X response curve, especially for particles smaller than 2.0 microns in diameter. Figure 5 shows the theoretical Mie curves calculated for different indices of refraction for the light scattering and collection geometry of the ASASP-X. Scanning electron micrographs have shown that the small particles in the flow train are nearly spherical. Larger particles are formed chiefly by agglomerations of small spheres, but the small particles of interest will scatter light according to Mie theory. Although Mie theory comprises assumptions such as an infinite plane wave source (that are not completely satisfied with the ASASP-X) it is the basis of operation of the instrument. Using different sized particles of known diameter (PSL particles) provides proper sizing, so the Mie scattering limitations do not affect the ASASP-X measurements.

PMS ASASP-X -- Air Flow

The PMS instrument extracts a sample of particle laden gas from the SEDS dilution chamber and surrounds it with a filtered sheath gas flow that aerodynamically focuses the sample to about 0.2 millimeters in diameter. The two flows are nearly matched isokinetically to prevent turbulent mixing in the sample chamber, thus avoiding divergence of the particles out of the laser beam. After passing through the laser beam, the sample and sheath flows are drawn from the sampling chamber, pass through a pump and a filter, and then split into two separate airstreams. The small airstream passes through the sample flow valve and meter and is exhausted. The large airstream passes through the sheath flow valve and meter and returns as the filtered sheath flow. This closed system monitors the sample flow at the exhaust while maintaining internally a closed loop of clean sheath gas. Figure 6 is a schematic of the ASASP-X airflow system.

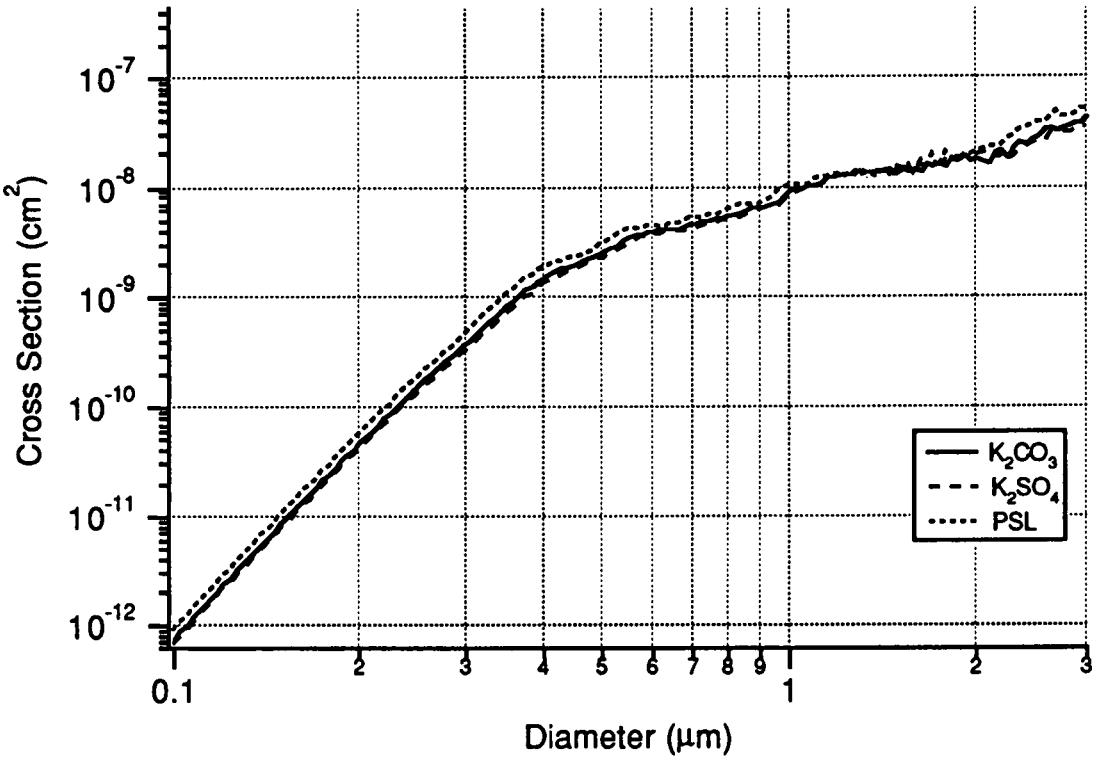


Figure 5. Calculated Mie Scattering Curves for the PMS ASASP-X [13].

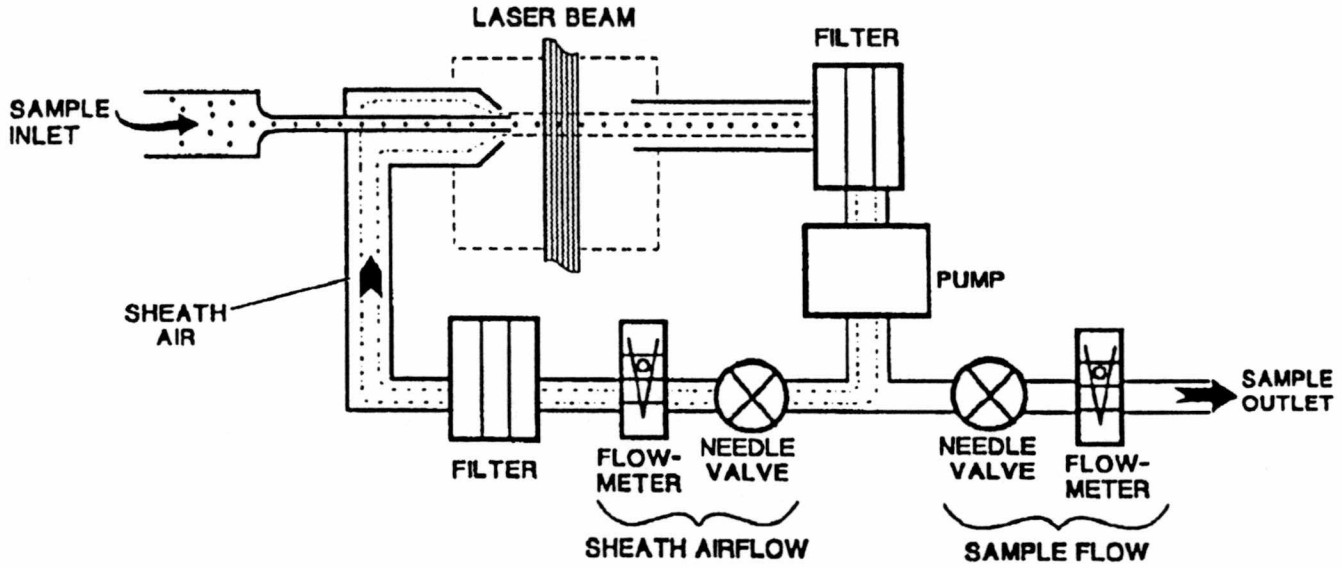


Figure 6. Airflow System of the PMS ASASP-X.

Source : Active Scattering Aerosol Spectrometer Probe, PMS Model ASASP-X Operating and Servicing Manual, Particle Measuring Systems, Inc., Boulder, CO Oct. 1991, page 6-2. Used with permission.

PMS ASASP-X -- Optical System

Since the particle sample flow is being contracted aerodynamically to 0.2 millimeters in diameter it is confined to the center third of a He-Ne laser beam operating in the TEM_{00} mode. Within the sample volume there is only a 15% variation in laser beam power. Because the particles pass through the laser cavity, the peak power of the incident radiation is about 30 watts. This high incident radiation power significantly enhances the resolution and accuracy of the instrument.

Scattered light is collected by a parabolic mirror positioned so that the particles scatter light from the paraboloid's focal point. This light encompassing 2π steradians of the total scattered radiation is thus collimated by the parabolic mirror and reflected from an angled flat mirror to an aspheric lens. The lens focuses the light onto a photodiode. The pulses of scattered radiation are individually analyzed and sized by a 32 channel pulse height analyzer. Figure 7 is a schematic of the ASASP-X optical system.

The ASASP-X is equipped with a feed back system that adjusts and compensates for varying laser power. At one end of the laser is a photodiode that constantly monitors the laser output. If the photodiode detects a decrease in laser intensity, the pulse height analyzer automatically adjusts. In this way, particles are sized correctly, even though laser power may be less than it was during calibration. When the laser power decreases significantly, the optics must be cleaned and the laser power must be peaked again. To avoid frequent cleaning of the mirrors, the ASASP-X could be modified to include purging of the mirror surfaces and the Brewster's window using liquid nitrogen.

Calibration of the instrument is done with particles of a known diameter. As particles scatter the laser light, potentiometers on the pulse height analyzer are adjusted. This calibration method allows the sizing uncertainty to be determined from the calibration variations and particle size variations.

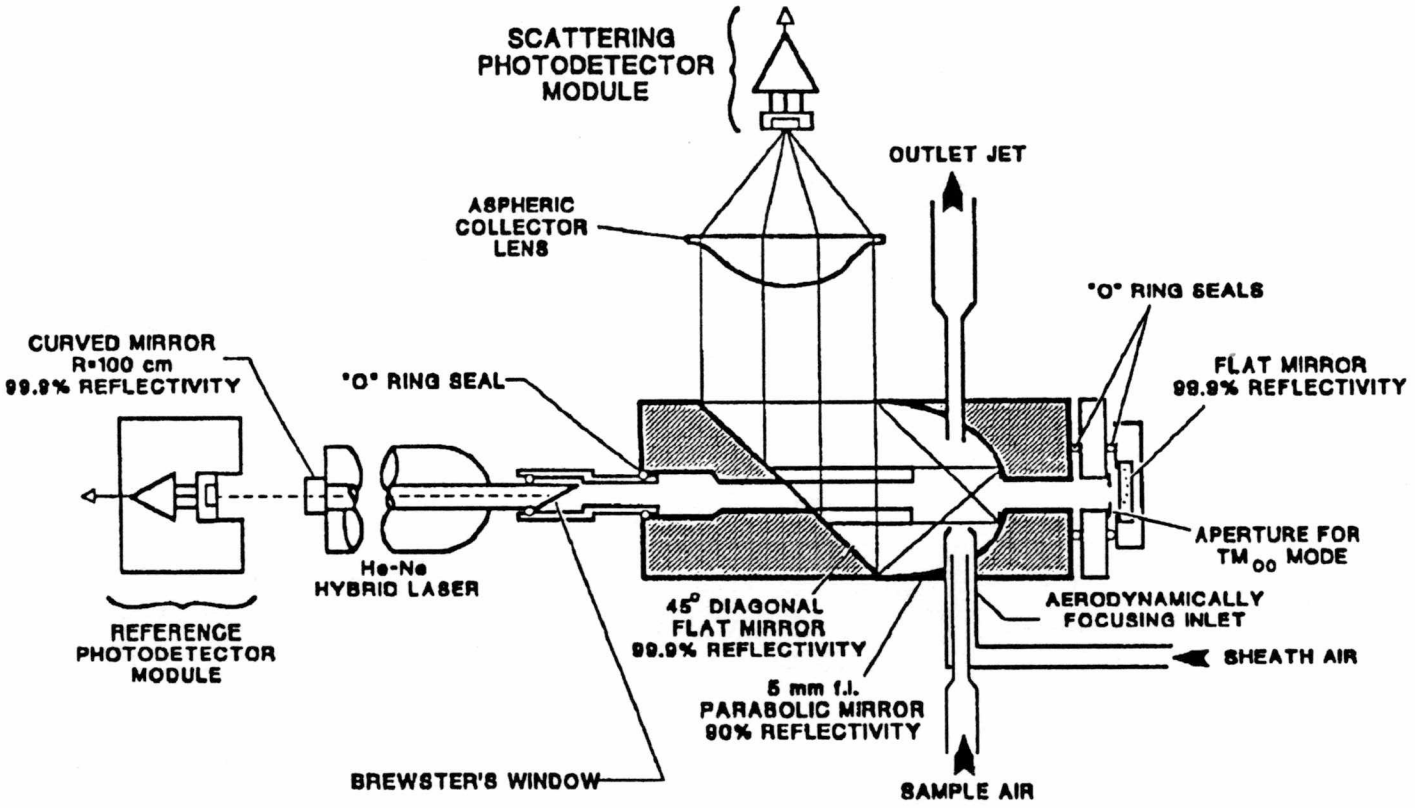


Figure 7. Optical System of the PMS ASASP-X

Source: Active Scattering Aerosol Spectrometer Probe, PMS Model ASASP-X Operating and Servicing Manual, Particle Measuring Systems, Inc., Boulder, CO Oct. 1991, page 6-5. Used with permission.

Advantages of the PMS ASASP-X

The PMS ASASP-X was the instrument of choice because it best fit the conditions typical of the CFFF environment. Optical analysis of particle sizes offered a much better particle size resolution than does aerodynamic analysis such as the 5 stage cyclone in the region of interest as is seen in table 1. The 32 particle diameter bin sizes range from 0.1 micron to 3.0 microns with one oversize bin. The oversize bin records all of the measurements of particles greater than 3.0 microns in diameter.

The adjustability of the sample flow rate allows for an increase in the maximum number density measurable by the instrument. The maximum number of particles per second the instrument's electronics can count is 20,000. The actual maximum number the instrument can accurately count in its standard configuration is 5,000 per second. This is due to the time of flight of each particle across the laser beam and due to the necessity of a high probability of only one particle at a time being in the sample volume. The maximum measurable number density is then:

$$\text{maximum density } \frac{\#}{cc} = \frac{\text{maximum count rate \#/sec}}{\text{sample flow rate cc/sec}}. \qquad (2)$$

The manufacturer's standard calibrated sample flow rate setting is 2.0 cc per second. If that flow rate is reduced to 0.2 cc per second and the instrument calibrated for that flow rate, the maximum measurable number density is 2.5×10^4 per cc. Combined with a SEDS dilution of 5000 to 1, the measurable number density could increase to about 10^8 per cc, which is the order of magnitude of the number density seen at the BH/ESP inlet. The filtered sheath flow must also be reduced to avoid turbulent mixing in the sample volume. As a result, the maximum measurable number density will be slightly less because the time of flight across the laser beam increases. However, the instrument's limit remains close to 5000 per second in this case also [14].

Table 1. Particle Size Ranges for Bins of the PMS ASASP-X.

Channel	Bin Size (microns)	Interval (microns)
1	0.10 - 0.11	0.01
2	0.11 - 0.12	0.01
3	0.12 - 0.13	0.01
4	0.13 - 0.14	0.01
5	0.14 - 0.15	0.01
6	0.15 - 0.16	0.01
7	0.16 - 0.17	0.01
8	0.17 - 0.18	0.01
9	0.18 - 0.20	0.02
10	0.20 - 0.22	0.02
11	0.22 - 0.24	0.02
12	0.24 - 0.27	0.03
13	0.27 - 0.30	0.03
14	0.30 - 0.35	0.05
15	0.35 - 0.40	0.05
16	0.40 - 0.45	0.05
17	0.45 - 0.50	0.05
18	0.50 - 0.60	0.10
19	0.60 - 0.70	0.10
20	0.70 - 0.80	0.10
21	0.80 - 0.90	0.10
22	0.90 - 1.00	0.10
23	1.00 - 1.20	0.20
24	1.20 - 1.40	0.20
25	1.40 - 1.60	0.20
26	1.60 - 1.80	0.20
27	1.80 - 2.00	0.20
28	2.00 - 2.20	0.20
29	2.20 - 2.40	0.20
30	2.40 - 2.70	0.30
31	2.70 - 3.00	0.30
32	> 3.00	

Another advantage of this instrument is its on-line, near real-time capability of analyzing a gas sample. The particle spectrometer continuously detects and analyzes particles in the gas and transmits the processed data to the computer serial port in time intervals ranging from 1 to 6553 seconds. Thus the ability of the ASASP-X to detect changes in particle size distribution and concentration is more than adequate for the CFFF, where significant changes typically occur over several seconds or minutes.

Aerodynamic vs. Optical Measuring

There are no commercially available particle sizing instruments with acceptable size resolution capable of measuring submicron particles with as high a concentration as seen at the CFFF, except for cyclones and impactors. These two devices do not have real-time capability or acceptable response time. There will be some differences between optical sizing measurements and standard aerodynamic measurements due to the variation in shape, index of refraction, and density of particles, which affect both the light scattering and the aerodynamic drag characteristics. Aerodynamic measurements made by the 5 stage cyclone will be taken as the standard; the deviation of particle size distribution measured by the SEDS will characterize the SEDS uncertainty. Repeating the 5 stage cyclone/SEDS comparisons several times will provide the basis for the calculation of bias and random uncertainty components.

Data Acquisition and Analysis

Data from the ASASP-X come through the serial port of a Macintosh computer as an array of 32 numbers, each number corresponding to the number of counts in a specific bin. The activity, defined as the percentage of time the instrument spends analyzing particles, precedes the data string. The activity includes both the transit event time and the processing time for all particle detection.

Data analysis is done on a Macintosh using National Instrument's LabVIEW® software. This allows for near real-time analysis of the particle loading and size distribution. When the string of data is received, the numbers are extracted and put into an array. Each array element corresponds to a single bin. Number densities are calculated by multiplying the array by the dilution ratio of the SEDS and dividing by the sample flow rate and sample time interval of the PMS instrument. The analysis and acquisition programs graph the data as number density (dN) normalized by bin width (dD) versus diameter (D). The graph updates with every new string of data received. Normalization of the number densities occurs before graphical display because the ASASP-X uses uneven bin sizes that cause the particle counts for each bin to be proportional to that bin size. When the measured particle size range and/or number counts span more than an order of magnitude, particle loading data are generally graphed on a log-log plot and normalized as $dN/d\log D$, where $d\log D$ is the logarithmic bin width, i.e., the difference of the logarithms of the bin limits:

$$D\log D = \log D_2 - \log D_1.$$

Data from 5 stage cyclone measurements are usually normalized with the base 10 logarithm. Insitec, Inc. used the natural logarithmic bin width. When used in comparison to 5 stage cyclone data or Insitec data, measurements taken with the SEDS are normalized accordingly.

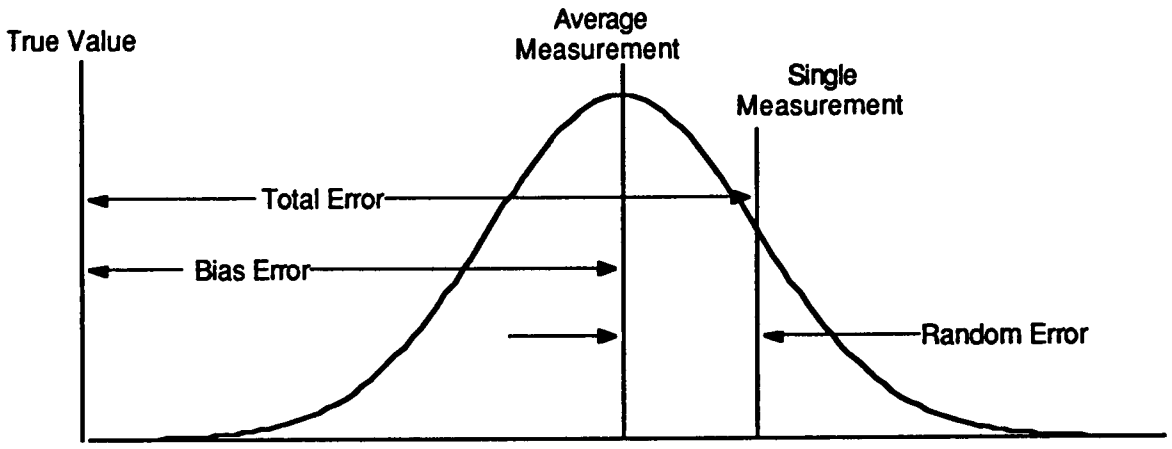
CHAPTER IV
Determination of Uncertainties

Nature of Error and Uncertainty

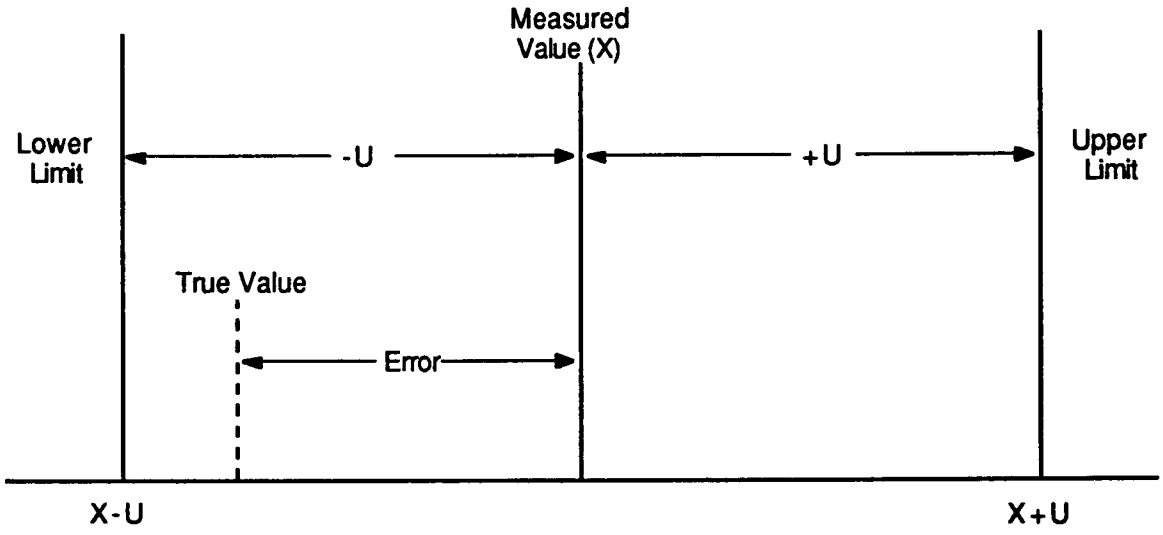
As stated in chapter III, the SEDS measures on-line, near real-time particle concentration distributions. However, the accuracy of the SEDS measurement is still unknown. As with any measurement, there will be uncertainties associated with the values reported by the SEDS [15]. Errors are the differences between the measured and the true value. The measurement error can be divided into a random error and a fixed bias error. The uncertainty interval is an estimate of the interval within which the true value will probably lie. For equal positive and negative bias uncertainties, the uncertainty interval is equal to twice the calculated uncertainty limit and is centered on the mean value measured. Figure 8 illustrates the concept of error and uncertainty.

5 Stage Cyclone

The overall uncertainty of measurements made with the SEDS is determined by comparing simultaneous measurements from the SEDS and the 5 stage cyclone taken at the BH/ESP inlet. Since the 5 stage cyclone measurements are assumed to be correct, the SEDS uncertainty will be the difference between the two measurements. The 5 stage cyclone measures number densities N_k (in particles per cc) by measuring the mass collected individually by each of the 5 stages and the final filter. The mass is converted to number counts by assuming the mass in each stage is due to M_k particles of uniform size, shape, and density. The particles are assumed to be spherical with diameters equaling the square root of the product of the bin limits (geometric mean diameter). The resulting counts are converted to particle concentrations by dividing the flue gas sample flow into the counts as



(a) Random and Bias Error in Relation to the True Value.



(b) Measurement Error and the Lower and Upper Uncertainty Limits of the Measurement.

Figure 8. Concept of Error and Uncertainty.

recorded by the 5 stage cyclone. The bin sizes of the 5 stage cyclone used at the CFFF are shown in table 2.

Several measurements for comparisons were planned to calculate the mean deviation (bias) and the standard deviation (random) uncertainty. The mean and standard deviation of the differences can be calculated with greater confidence as the number of measurements increases.

Insitec Inc.

As another independent test with greater size resolution, measurements were done simultaneously with the PCSV-UFP from Insitec, Inc. The PCSV-UPF is also a single particle counter employing Mie theory. Particles scatter light as they pass through a sample volume formed by focused laser light. The particle size is determined by the maximum amplitude of scattered light using a response function based on Mie theory. The response function is coupled with a deconvolution technique using the spatial intensity variation in the sample volume to remove the dependency of the measured particle size on the particle's trajectory. Two laser beams are used to measure sequentially a size distribution. The measurement results are concatenated during data reduction to determine the size distribution.

Since the lower measurement limit of the Insitec PCSV instrument is about 0.9 microns in the high loading environment at the BH/ESP inlet, a calibration rig was used to create a lower number density environment for SEDS versus PCSV calibration experiments. These experiments were done while the SEDS was sampling at different dilutions to find the effect of different dilution ratios on the size distribution measurements.

In the calibration rig, ash collected from the electrostatic precipitators at the CFFF was injected through a sandblast nozzle into the lower end of an 18 foot length of 3 inch diameter PVC pipe mounted vertically. The ash was mixed with air supplied from the opening in the bottom of the pipe, drawn upward and exhausted into the flue by suction

Table 2. Bin Sizes of the 5 Stage Cyclone

Stage	Size Range in Microns
Filter	< 0.28
5	0.28 - 0.56
4	0.56 - 1.4
3	1.4 - 2.0
2	2.0 - 4.0
1	> 4.0

provided by the flow train at the CFFF. The Insitec probe and the SEDS probe were located on the BH/ESP inlet platform where the sampling took place. Figure 9 is a schematic of the calibration rig. The particle concentration was varied by controlling the injection rate of the sandblast gun. Comparisons between the SEDS and Insitec measurements will provide an uncertainty calibration as a function of SEDS dilution rates, assuming that the errors in the Insitec probe measurements are small. Measurement uncertainties of the Insitec probe will be made by comparing the probe's results to the 5 stage cyclone measurements. These Insitec versus 5 stage cyclone comparison measurements were made at the BH and DESP outlet, where particle concentrations are low enough to allow the PCSV to measure particles of less than 0.3 microns in diameter.

SEDS Uncertainty -- Experimental

The SEDS calculates particle concentrations in the flue gas by the formula

$$N_j = \frac{M_j Z_j}{Rt}, \tag{3}$$

where

N_j is the number density (particles per cc),

M_j is the number as measured by the PMS instrument,

Z_j is the dilution ratio of the SEDS,

R is the PMS instrument sample flow rate (in cc per second),

t is the PMS instrument time interval (in seconds) during which particles are counted, and

j is the array index corresponding to a PMS instrument bin size.

Since the total uncertainty is a combination of both the bias uncertainty and the random uncertainty, measurements were repeated many times to estimate a bias and

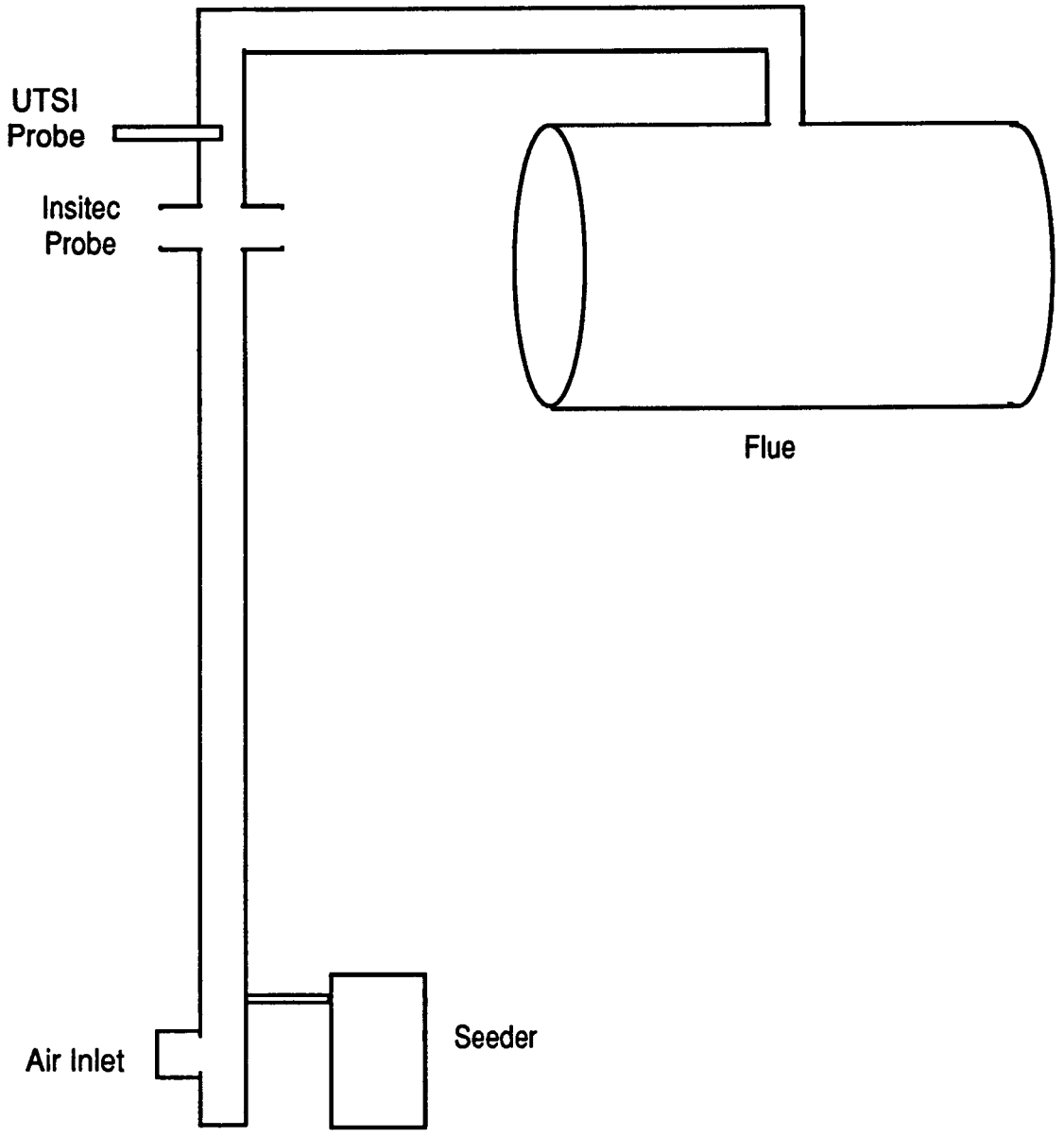


Figure 9. Schematic Diagram of Calibration Rig Used for Simultaneous Experiments with Insitec, Inc.

standard deviation. Using the 5 stage cyclone as the standard, the total bias estimate B will be the average of the measurement differences:

$$B = \frac{1}{n}\sum_{i=1}^{n} \Delta_i, \tag{4}$$

$$\Delta_i = N_{cyclone} - N_{SEDS}, \tag{5}$$

where

N_{SEDS} is the number density as measured by the SEDS, as a cumulation of all the particles in the bins that overlap the 5 stage cyclone bin,

$N_{cyclone}$ is the number density as measured by the 5 stage cyclone, and

n is the total number of comparison measurements made.

The random error estimate S will be the standard deviation of the measurement differences:

$$S = \sqrt{\frac{\sum_{i=1}^{n} [(\Delta_i - B)^2]}{n-1}}. \tag{6}$$

The uncertainty limit is defined as

$$U = \sqrt{B^2 + (t_{95}S)^2}, \tag{7}$$

where t_{95} is Student's t parameter at the 95% confidence level. Since large numbers of measurements were taken, the statistical distribution will be gaussian; the value 2 was used for t_{95}. Separate B, S and U values can be defined for each 5 stage cyclone stage that overlaps the SEDS measurements (the filter and stages 5, 4, and 3). The resulting bias, random error, and uncertainty values can be combined to determine the overall SEDS

measurement uncertainty. Similar comparisons were done with measurements from the PCSV.

SEDS Uncertainty -- Theoretical

The uncertainty of the SEDS measurement is an accumulation of the measurement uncertainty of the individual measurement components. To reduce the measurement uncertainty of the SEDS, minimization of the most influential factors needs to be addressed. By expanding the particle concentrations (equation (3)) in a Taylor series, the influence of the different components of random and bias uncertainty can be found. Expanding the expression for N_j about the true values q gives:

$$N_j(x) - N_j(q) = \sum_{i=1} (x_i - q_i)\frac{\partial N_j}{\partial x_i} + \text{higher order terms}, \tag{8a}$$

$$\frac{\partial N_j}{\partial x_i} = IC_x, \tag{8b}$$

where (x_i - q_i) represents either the mean (bias) or standard deviation (random or precision) uncertainties of the measured values of M_j, Z_j, R, and t. The right hand side of equation 8a expresses either the random or the bias uncertainty on N_j as a function of the random or bias uncertainties in M_j, Z_j, R, and t. The higher order derivative terms are taken to be small, so they are generally ignored. IC_x is the influence coefficient for the variable correspending to x_i.

The root-sum-square method has been shown to give a good estimate of the total bias and standard deviation of the component uncertainty when there are several contributing components [15]. Summation of contributing components will overestimate the component uncertainties since it is unlikely that all components will reach their limiting value. The root-sum-square method defines the component bias uncertainty as,

$$B = \sqrt{\sum_{i=1} \beta_i^2}, \tag{9a}$$

where β_i is an estimate of the bias error from one elemental source i, and the component random uncertainty is:

$$S = \sqrt{\sum_{i=1} \sigma_i^2}, \tag{9b}$$

where σ_i is the estimate of the experimental standard deviation from one elemental source i.

The calculated component uncertainties are propagated through the Taylor series expressions to calculate a total bias B and total random uncertainty S:

$$B = \sqrt{\sum_{i=1} \left[\left(\frac{\partial N}{\partial x_i} B_i \right)^2 \right]}, \tag{10a}$$

$$S = \sqrt{\sum_{i=1} \left[\left(\frac{\partial N}{\partial x_i} S_i \right)^2 \right]}. \tag{10b}$$

For the particle number density N, the total bias B and random error S is

$$B = \sqrt{\left(\frac{Z}{Rt} B_M \right)^2 + \left(\frac{M}{Rt} B_Z \right)^2 + \left(-\frac{MZ}{R^2 t} B_R \right)^2 + \left(-\frac{MZ}{Rt^2} B_t \right)^2}, \tag{11a}$$

$$S = \sqrt{\left(\frac{Z}{Rt} S_M \right)^2 + \left(\frac{M}{Rt} S_Z \right)^2 + \left(-\frac{MZ}{R^2 t} S_R \right)^2 + \left(-\frac{MZ}{Rt^2} S_t \right)^2}, \tag{11b}$$

and the limit of the total uncertainty of the measurement will be as in equation 7. The bias and random uncertainties in equations 11 are evaluated for values of M, Z, R, and t corresponding to a value of N typical for SEDS operation at the CFFF; this provides the uncertainty of the SEDS at that operating condition.

Evaluation of Uncertainty Due to Individual Components

This section details the plan to determine the uncertainty contribution that each of the components in equation 3 has on the overall uncertainty. Controlled experiments were conducted to define the biases and the random spread of each component's measurements. Separate sizing uncertainty measurements were made for the particle counters with repeated detailed calibration of the instruments using particles of a known size. Once the component uncertainties are determined, the overall uncertainty is calculated employing equations 7 and 11. This overall uncertainty in measurements made with the SEDS is compared to the uncertainty measurements made with the 5 stage cyclone.

Time Interval

The variable t is the time interval during which particles are counted. Its uncertainty is the uncertainty of the clock of the ASASP-X. The ASASP-X is timed with a standard 2.4576 MHz clock [16], resulting in a maximum random uncertainty of ± 1 clock pulse, or $\pm 4.069 \times 10^{-7}$ sec. The bias uncertainty in t is the deviation of the clock from the true frequency and is estimated to be at ± 100 ppm ($\pm 10^{-4}$ seconds). This is a typical frequency tolerance for a 2.46 MHz clock oscillator [17].

Sample Flow Rate

R is the sample flow rate of the particle spectrometer. This flow rate determines how many particles per time interval pass through the ASASP-X laser beam to be counted. To control and monitor the flows, the instruments use mass flow rotometers. To determine an accurate volumetric flow rate through the rotometers, the volume of air passing through the meter at a given setting was measured with a secondary standard pipette flow meter. A graduated pipette was connected to the outlet of the flow meter, and the volumetric flow rate was determined by timing the flow of a soap bubble through the pipette. This method is the accepted standard method for calibrating low volume flow meters. The uncertainties

in the pipette flow meter are several orders of magnitude better than the typical 5% repeatability of rotometers. It provides an accurate measure of the uncertainties in the rotometer sample flow rate. The pipette was calibrated to 0.1cc. The stop watch used with the system was accurate to 0.01 second. The bias uncertainty of the pipette is estimated to be

$$B = \sqrt{\left(\frac{1}{t}\Delta V\right)^2 + \left(\frac{V}{t^2}\Delta t\right)^2}, \tag{12}$$

where

V is the volume through which the soap bubble passed, and

t is the measured time for the soap bubble to pass through the volume.

This uncertainty is all bias since, as with all calibration, the uncertainty components propagate as a fossilized bias [15].

Rotometers respond to the momentum of the gas passing through them rather than volume, so it is necessary to determine the uncertainties in these volumetric flow rates at operating conditions, since these conditions may alter the flow of gas through the rotometers. The bubble experiments were therefore carried out while the instruments were drawing samples from the SEDS vacuum chamber, as this is the normal operating mode of the PMS instruments in the SEDS. Experiments were not conducted at significant changes in gas temperature because the SEDS gas coolers will maintain a near constant gas sample temperature.

Bias uncertainties and random uncertainties were calculated in the normal way:

$$B_R = \frac{1}{n}\sum_{i=1}^{n}(R_i) - R_o, \tag{13a}$$

$$S = \sqrt{\sum_{i=1}^{n}\left[\frac{(R_i - \langle R\rangle)^2}{n-1}\right]}, \tag{13b}$$

where

n is the number of tests done,

R_i is the measured flow rate for test i,

$\langle R \rangle$ is the average flow rate measured, and

R_o is the nominal flow rate.

The additional uncertainties in the pipette flow meter are so small that their contribution is insignificant to the rotometer uncertainties, and they were ignored.

Correction Factor

While doing measurements with both ASASP-X instruments, sample flow rates as monitored by the rotometers were observed to vary with time. Despite the care taken to set and maintain proper flows, temporal variations occurred, usually as both small oscillations around the set calibrated value and a small gradual drift up or down from the set point to a quasi-stable flow. Small differences in the sample flow rate significantly affect the number of particles seen by the ASASP-X when a high particle loading is being measured, and so these flow fluctuations greatly influence the loading uncertainties.

With the two instruments sampling simultaneously from the same source without dilution, and careful attention is paid to setting and maintaining proper sample flow rates, the calculated number densities should be equal. When they are not equal, the cause can be attributed to variations in the flow rates R_1 and R_2. At this point a correction factor α can be introduced into the equation that will cause N_1 to equal N_2:

$$N_1 = \frac{M_1}{\alpha R_1 t_1} = N_2 = \frac{M_2}{R_2 t_2}. \tag{14}$$

To find the value of α, a large number of measurements were taken with both instruments simultaneously sampling polydisperse particles (room dust or fly ash in the form of K_2CO_3) from the same location in space. A ratio of the array of calculated number

densities gave the correction factor α in each particle size counting bin. To attain reasonable statistical confidence in the α values determined, only those bins with a significant number of counts for both particle sizing instruments were used. An average over all of those usable bins gives a mean value of α for the size distribution curve. If a large number of data sets are taken and an α calculated for each one, then the bias and standard deviations of α can be calculated.

The uncertainties associated with α actually become uncertainties in the sample flow rate R since the actual flow rate will be the product of the nominal value of R and its correction factor α.

The procedure to calculate the error in α can be illustrated by considering a single data set i. A ratio of the calculated number densities of data set i and bin size j gives a value of α_{ij}'s from equation 14:

$$\alpha_{ij} = \frac{N_{1_{ij}}}{N_{2_{ij}}}. \tag{15}$$

α_{ij} is the correction factor needed to correct bin j in one data set i. If the sample flow rates were set at the proper values and were steady throughout the duration of the sampling time, then α_{ij} would be one. There is the possibility of α_{ij} being equal to zero or infinity. Only in cases where the correction factor is near 1 ($0.7 < \alpha_{ij} < 1.3$), the data is not used. A more thorough discussion of this is in chapter V.

Averaging over all of the significant bins produces one α_i for the data set i:

$$\alpha_i = \frac{1}{n} \sum_{j=1}^{n} \alpha_{ij}, \tag{16}$$

where n is the number of bins to be averaged. The value of the number n is taken such that all bins smaller than n have at least 1000 particle counts. The 1000 was arbitrarily chosen

to achieve a high statistical confidence. α_i is now a number that can be multiplied by N_{2i} that would correct for the variable flow rates over the data set i. Using this average α_i, a bias uncertainty and standard deviation uncertainty in the flow rate variation of data set i can be calculated. The bias is the difference of the average over all data sets ℓ and the nominal value α_o, and the random uncertainty is the standard deviation of the ℓ measurements. Thus,

$$B_\alpha = \frac{1}{\ell}\left(\sum_{i=1}^{\ell} \alpha_i\right) - \alpha_o, \tag{17}$$

$$S_\alpha = \sqrt{\sum_{j=1}^{\ell}\left[\frac{(\alpha_i - \langle\alpha_i\rangle)^2}{\ell - 1}\right]}. \tag{18}$$

To take the sample of room dust, both probes sampled simultaneously from the same place in space. This was done by connecting ¼ inch tubing to the inlet of each instrument and running both tubes to a common tee. The tubing was about 4 feet long, since that is the same length that is required to connect the PMS ASASP-X to the SEDS.

Sampling of the fly ash was done by blowing the ash through a sandblast gun with compressed air. A short rubber hose directed the ash to a sample duct. This sample duct consisted of a piece of Plexiglas tube 19 inches long and 6 ½ inches in diameter. A fan was set near the inlet of the duct to enhance mixing of the particles in air. Halfway into the duct, a 1 ¼ inch thick honeycomb flow straightener was set to improve spatial uniformity of the particle dispersion. The sample probes were suspended near the center of the exhaust end of the duct. A schematic of this sample duct is in figure 10.

Since ultimately measurements are done while the PMS instrument samples from the vacuum of the SEDS mixing/sample chamber, a vacuum chamber was made identical to that of the SEDS. Both room air and fly ash fluidized by the above described duct were drawn into the chamber which was maintained at an appropriate negative pressure (10 to 30 inches of water below atmospheric pressure). The spectrometers then sampled from a

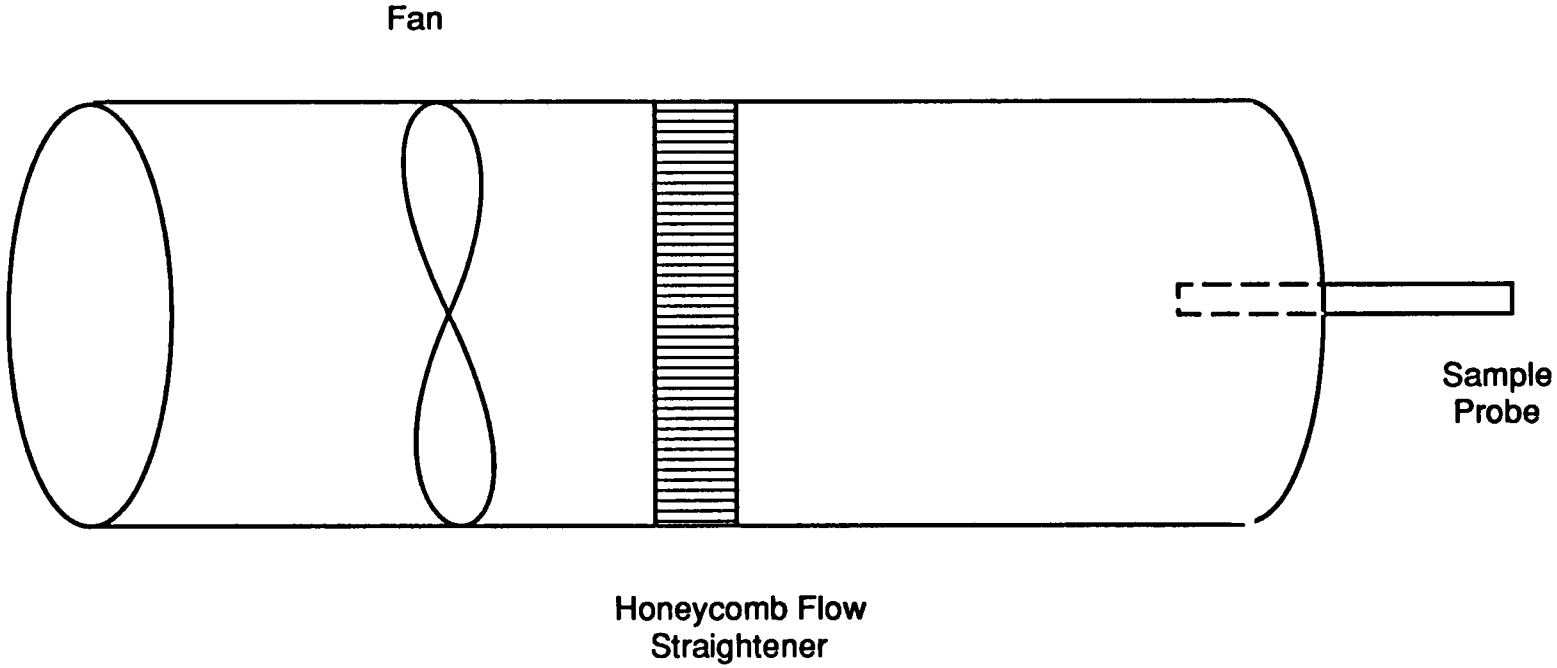


Figure 10. Schematic Diagram of Sample Duct Used for Collection of Fluidized Ash Particles.

single probe set into the vacuum with a tee on the outlet to provide simultaneous sampling for both instruments.

Event Counts

M_j is the actual number of particles counted by the ASASP-X during the time interval t and placed in bin j corresponding to a bin size listed in table 1. When the ASASP-X operates properly, the uncertainty in M_j is due chiefly to the ability or inability of the PMS instrument to correctly account for a particle.

Monodisperse (single diameter) particles were used to verify the accuracy of the instruments to correctly size the particles. Polystyrene latex (PSL) particles were purchased from Duke Scientific Corporation with diameters of 0.121 microns, 0.222 microns, 0.451 microns, and 0.913 microns. The standard deviations in these particle diameters were given as 0.0050 microns, 0.0038 microns, 0.0113 microns, and 0.0059 microns, respectively. To suspend the spheres in air, one or two drops of the concentrated 10% solid particle solution was mixed with 500 ml of deionized, distilled water. This solution was put into a plastic pharmaceutical nebulizer where the particles became airborne in filtered air. They were mixed with more filtered air in a drying chamber from which they were extracted and measured by the PMS instruments. Figure 11 shows the nebulizer experimental set up. The tubing consisted of ¼ inch plastic tubing and a plastic hose 1 inch in diameter. Flow rates through the rotometers were about 7 standard cubic feet per hour (scfh) through the drying air and about 25 scfh through the nebulizer.

The drying chamber was a 7 foot length of 4 inch diameter PVC pipe with several bends as seen in figure 12. The sampling probes for the PMS spectrometers were about 10 inches long and set about 2 feet downstream from the inlet of the drying chamber such that their openings were in the center of the pipe diameter. At the end of the PVC pipe, a small exhaust hole was drilled. To prevent contamination with room aerosol, there was no other opening in the tube.

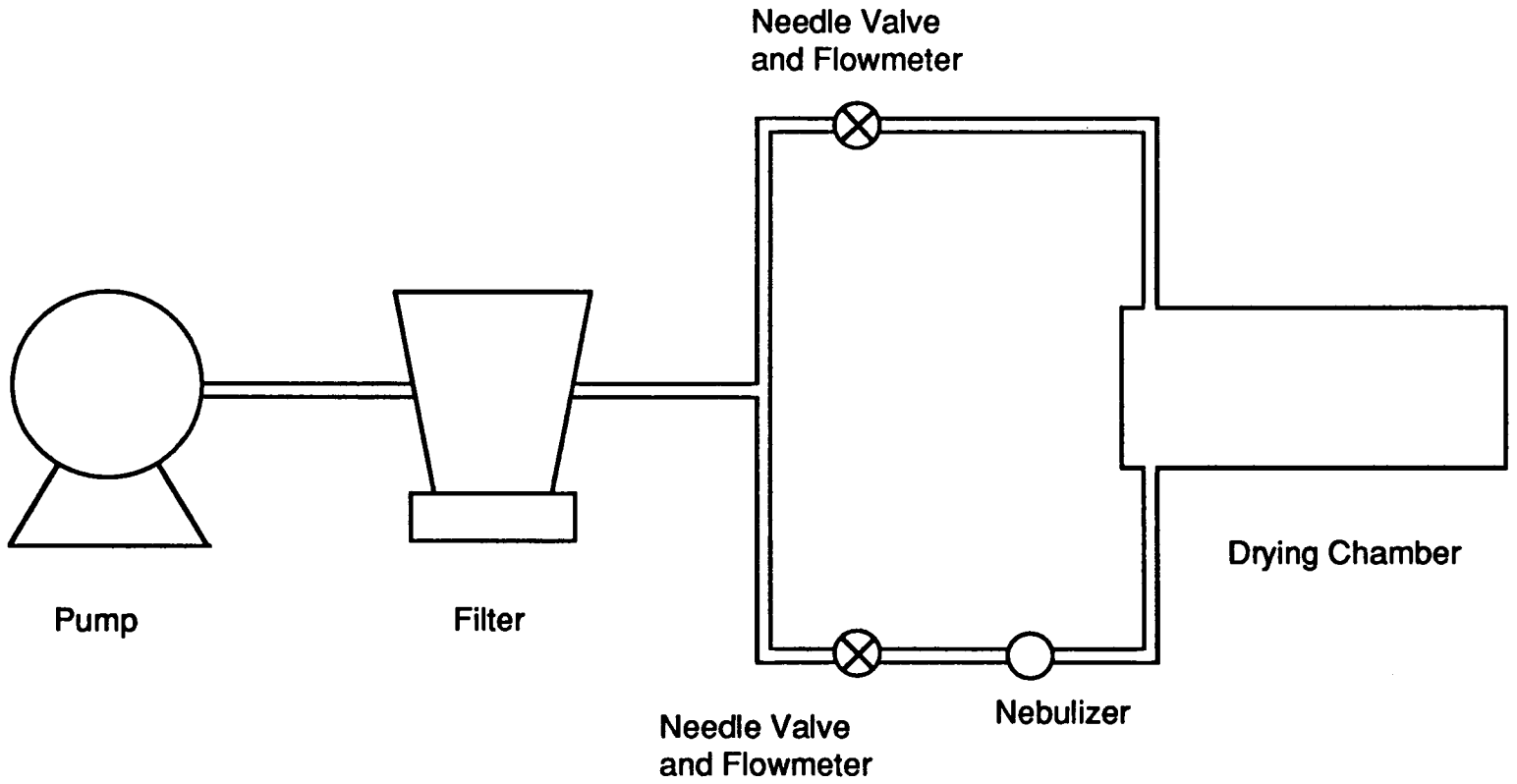


Figure 11. Schematic Diagram of Nebulizer System.

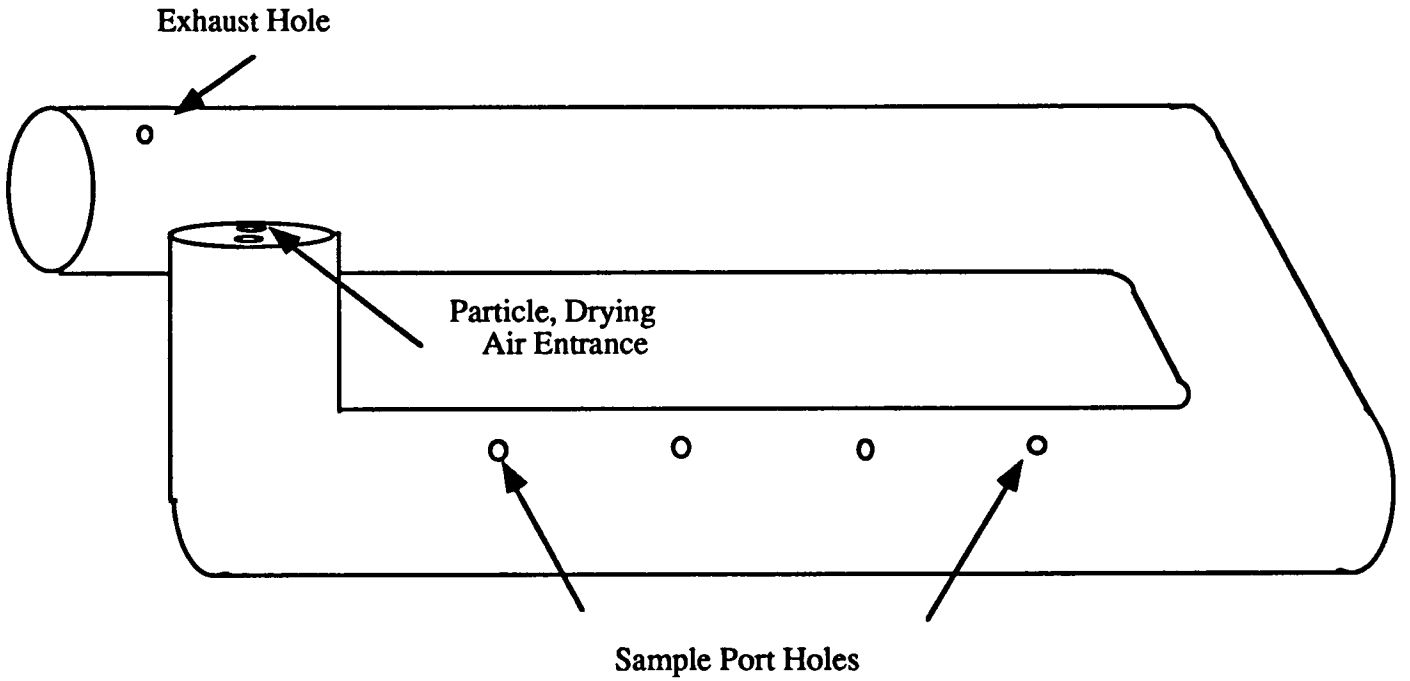


Figure 12. Schematic Diagram of Drying Chamber Used with Nebulizer System.

The bias and standard deviation uncertainty of M_j are found by sampling the PSL particles with the ASASP-X. The instrument, when working properly, places particles in the correct bin size but with some spread from the nominal particle size. Each bin puts a fraction of its own particles into neighboring bins but also receives a fraction of its neighbor's particles. If the two adjacent bins have nearly the same absolute number, then the recorded count in that bin should be very near the actual number of particles with that particular size. Therefore, the error in placing particles is minimal, but only if the ASASP-X places particles equally in both smaller and larger bins. However, when adjacent bins are very different in the absolute number count, a bias and a random uncertainty exist. These values can be calculated from the PSL measurements in the normal way:

$$B_m = \langle D \rangle - D_o, \tag{19}$$

$$S_m = \sqrt{\frac{\sum_{i=1}^{n} [(D_i - \langle D \rangle)^2]}{n-1}}, \tag{20}$$

where

$\langle D \rangle$ is the average of the diameters measured,

D_o is the nominal particle diameter, and

n is the number of particles under the curve of interest.

By determining the uncertainties in this manner, the variation in the PSL calibration particles' diameters will be included.

Dilution Ratio

Z_j is the dilution factor of the SEDS. The uncertainty involved with Z_j involves all of the parameters associated with various pressure drops, temperatures, and orifice calibrations. The dilution Z is also an array of 32 elements, since different particle sizes may dilute nonuniformly.

The theoretical dilution factor is given by the formula [6]

$$Z = \frac{K_L \sqrt{P_L / T_{R_L}}}{K_S \sqrt{P_S / T_{R_S}}} \frac{(\Delta P_L)^{b_L}}{(\Delta P_S)^{b_S}} \sqrt{\frac{mw_{dry}}{mw_{wet}}}, \tag{21a}$$

$$P = BP + P'/13.6, \tag{21b}$$

$$mw_{dry} = \left(\frac{mw_{wet} - mw_{H_2O} \times f}{1 - f} \right), \tag{21c}$$

$$T_R = T_F + 459.67, \tag{21d}$$

where*

L denotes the dilution air (large) orifice,

S denotes the sample air (small) orifice,

K = orifice calibration constant,

P = absolute pressure at high side of the orifice in inches of water,

BP = barometric pressure in inches of mercury,

P' = static pressure at high side of the orifice in inches of water,

ΔP = pressure drop across orifice in inches of water,

T_R = absolute temperature of gas in the orifice (Rankine scale),

T_F = temperature of gas in the orifice (Fahrenheit scale),

mw_{dry} = dry molecular weight of the carrier gas,

mw_{wet} = wet molecular weight of the carrier gas,

mw_{H_2O} = molecular weight of water,

f = mass fraction of water in the sample, and

b = parameter to best fit the calibration curve obtained experimentally.

* A table of conversions to MKS units can be found in the 72nd edition of the *CRC Handbook of Chemistry and Physics*, pages 1-19 to 1-36.

By substituting the expressions for P, T_R, and mw_{dry} into equation 21a, we get

$$Z = \frac{K_L}{K_S}\sqrt{\left(\frac{BP + P_L'/13.6}{BP + P_S'/13.6}\right)\left(\frac{T_{F_S} + 459.67}{T_{F_L} + 459.67}\right)\left(\frac{1-(mw_{H_2O}/mw_{wet})f}{1-f}\right)}\frac{(\Delta P_L)^{b_L}}{(\Delta P_S)^{b_S}}. \quad (22)$$

A Taylor's series expansion of this equation about its nominal values will give a value of the expected limit on uncertainty associated with D:

$$B_Z = \sqrt{\sum_{i=1}\left[\left(\frac{\partial N}{\partial x_i}B_i\right)^2\right]}, \quad (23a)$$

$$S_Z = \sqrt{\sum_{i=1}\left[\left(\frac{\partial N}{\partial x_i}S_i\right)^2\right]}, \quad (23b)$$

where B_i and S_i are the bias and random error of the parameter under consideration.

The bias and standard deviation uncertainties for each component of Z_j come from the several manufactures' specifications on all monitoring instruments (pressure transducers, thermocouples) with the exception of the orifice constant K and the calibration curve fitting constant b. These values were determined by the orifice equation [6]:

$$Q = K\sqrt{\frac{Pmw}{T_R}}(\Delta P)^b, \quad (24)$$

where

Q is the mass flow rate in grams per minute, and

mw is the molecular weight of the carrier gas (air in the calibration).

All other variables in equation 24 are previously defined. To calculate the values of K and b and their respective uncertainties, several data points were taken using known flow rates,

pressures, and temperatures. The value of parameters and their standard deviations were determined by fitting the data to the curve described by equation 24. The bias uncertainty of K will be calculated by holding b constant, and using the data points for Q, P, ΔP, m, and T_R, to solve for several K's. When a set of K's has been calculated, the bias will be calculated by taking the difference between the average of these K's and the curve fitted K.

$$\langle K \rangle = \frac{1}{n} \sum_{i=1}^{n} \left(Q_i \sqrt{\frac{T_{R_i}}{mP_i}} \frac{1}{\Delta P^{b_{calc}}} \right), \tag{25a}$$

$$B_K = \langle K \rangle - K_{calc}. \tag{25b}$$

A similar calculation will be used to find the bias of b:

$$\langle b \rangle = \frac{1}{n} \sum_{i=1}^{n} \left[\frac{\ln \left(Q_i \sqrt{\frac{T_{R_i}}{mP_i}} \right) - \ln (K_{calc})}{\ln (\Delta P_i)} \right], \tag{26a}$$

$$B_b = \langle b \rangle - b_{calc}. \tag{26b}$$

The results of the uncertainty measurements and calculations are deferred to chapter V. First the overall uncertainty is discussed in experiments with the 5 stage cyclone. This is followed by a description of the experimental work done to find the individual contributions to the overall uncertainty. Finally the numerical results are presented.

CHAPTER V
Uncertainty Results

Overall Uncertainty: vs. 5 Stage Cyclone

Figure 13 shows typical data collected from the BH inlet by the 5 stage cyclone. These are typical numbers that would be used to check the SEDS calibration. However, during LMF5 testing, operational problems were encountered. First gradual plugging occurred within the SEDS. Figure 14 shows the number density as measured with the SEDS decreasing with time. In an attempt to eliminate plugging, the dilution orifice was changed to a larger one to allow higher flow that would keep the system from plugging. However, for increased flow the dilution was lower and too many particles were entering the instrument's sample volume; the instrument was overwhelmed.

The PMS ASASP-X monitors its particle detection and analysis time. The manufacturer recommends that the instrument's activity be kept below 20% to ensure linear response. When there are many particles in the sample cavity and the activity is above 50%, events are missed. Also, the size distribution shifts to larger bin sizes as the activity increases. Smaller particles are masked out because the small particle channels see a continuous high level and rarely reset to measure small particles. Figure 15 displays how the small size bins become masked while large size bins have increased counts with increasec activity.

The problem in the SEDS became one of how to have a small enough sample flow through the system to ensure high dilution while using a large enough orifice to keep the system from plugging. The sample orifice was redesigned by moving the pressure tap from far downstream to the vena contracta, as shown in figure 16. By moving the tap to the vena contracta, figure 17 [18] shows that the maximum pressure difference occurs across the orifice. The low sample flow can be accurately measured with a larger orifice.

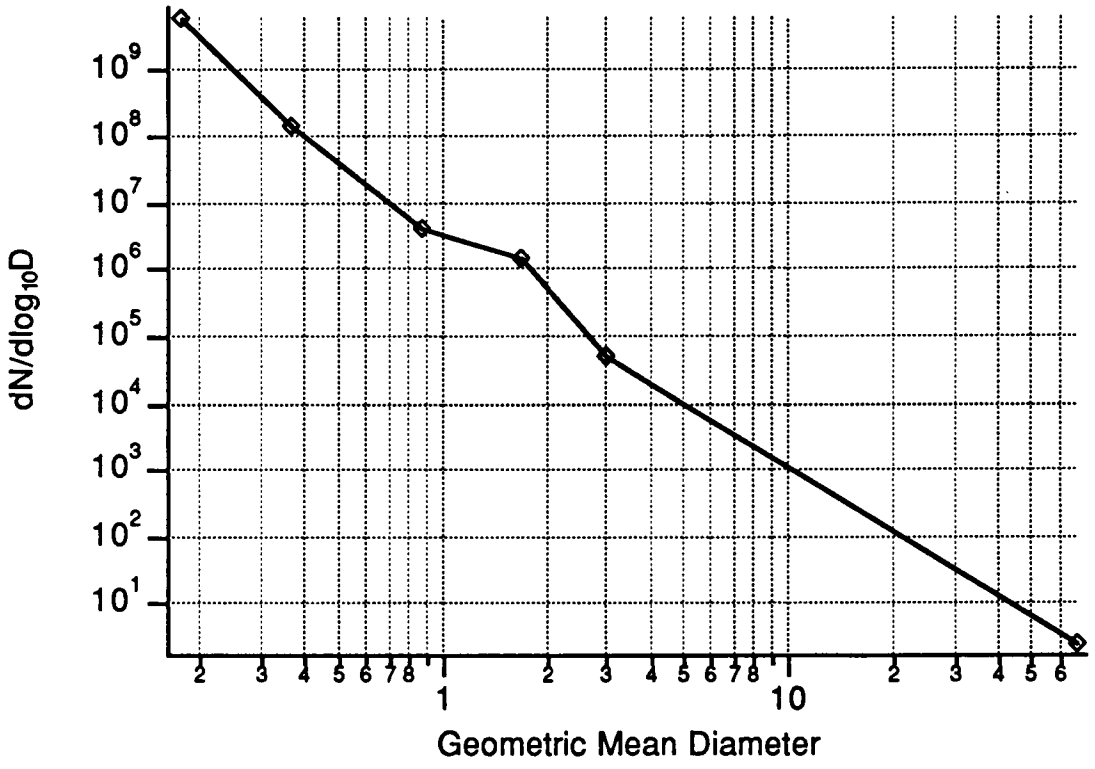


Figure 13. Typical Data Collected by the 5 Stage Cyclone at the BH/ESP Inlet.

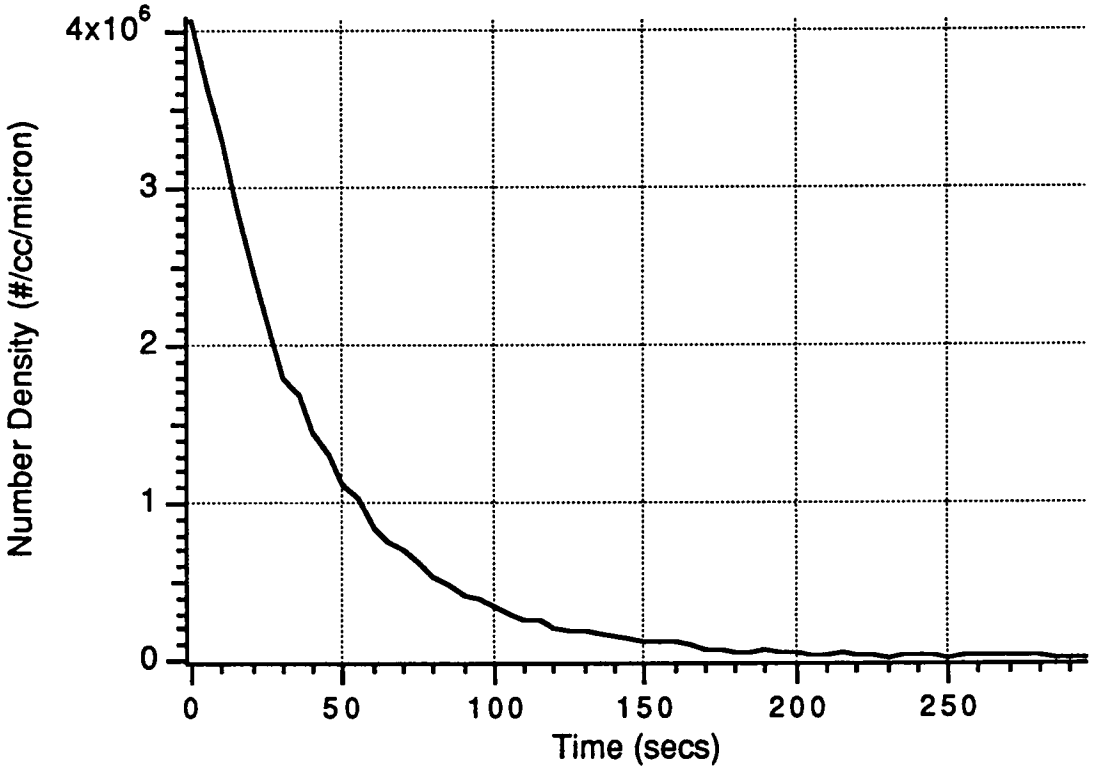
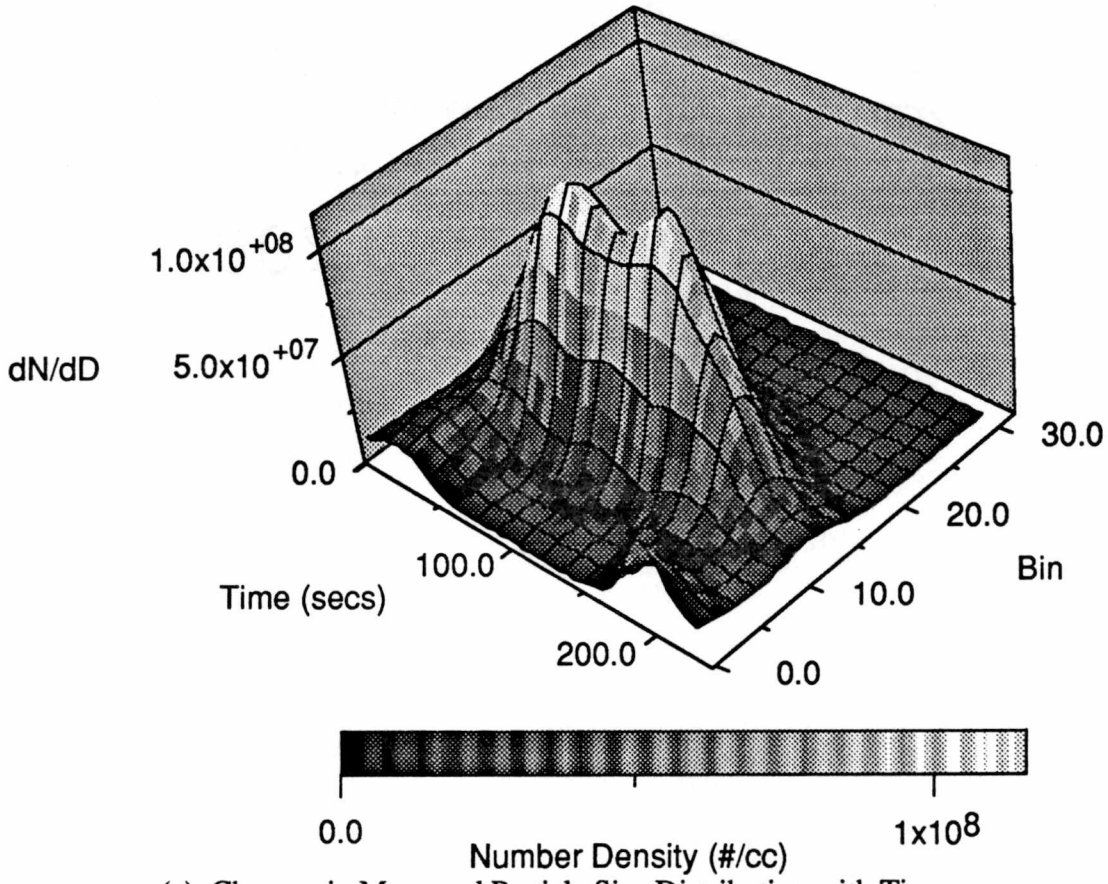
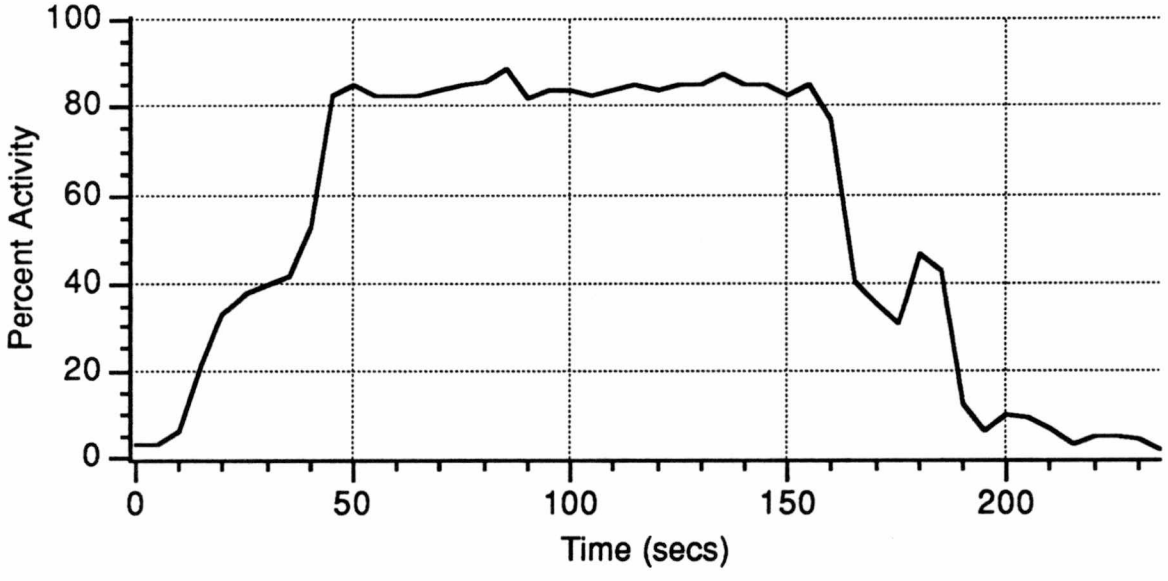


Figure 14. Total Number Density as Measured Through the SEDS Decreasing with Time.

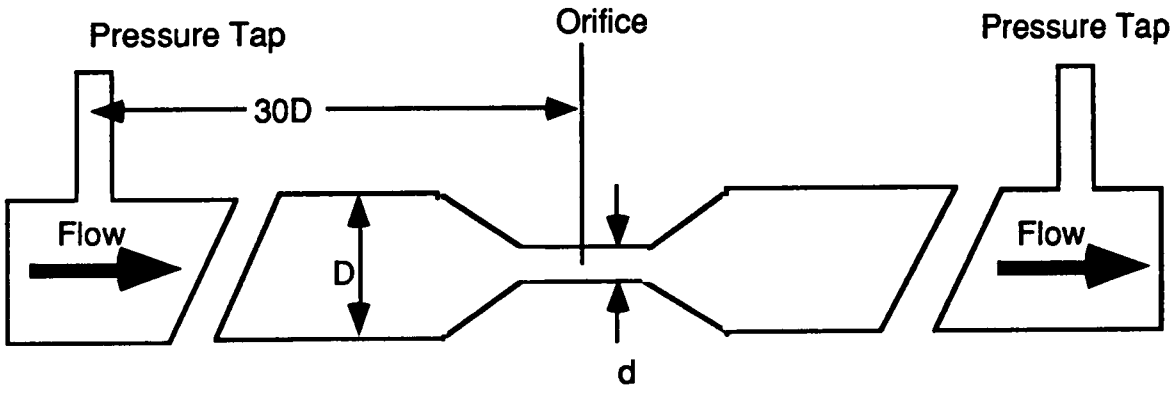


(a) Changes in Measured Particle Size Distribution with Time.

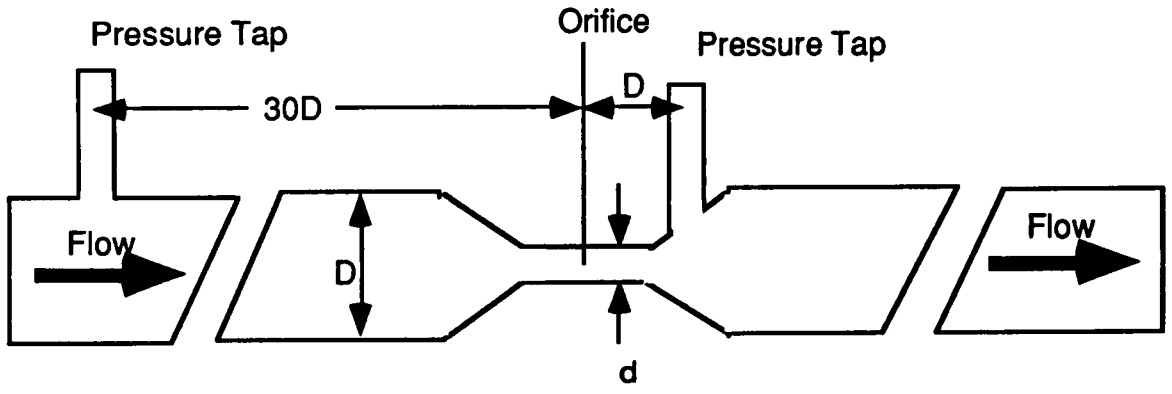


(b) Corresponding "Percent Activity" of Particle Spectrometer

Figure 15. Correspondence of Particle Concentration Distribution and Activity of Particle Spectrometer with Time.



(a) Original Design.



(b) Redesign

Figure 16. Schematic Diagram of Sample Orifice in SEDS.

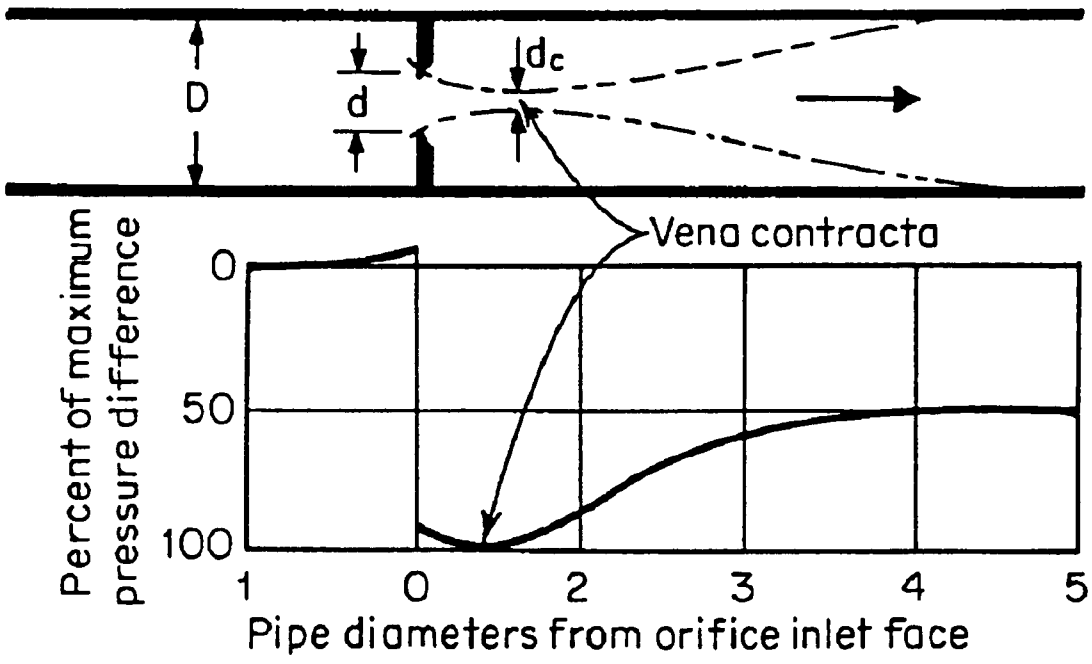


Figure 17. Relative Pressure Changes Due to Flow Through an Orifice [18]

Source: *Mark's Standard Handbook for Mechanical Engineers, Eighth Ed.*, Baumeister, T., Editor, McGraw-Hill Inc., New York, 1978, pp. 3-63. Used with permission.

Measurements made with this configuration still did not improve results. The SEDS continued to show plugging. When the orifice was removed, it did not appear to be plugged, which suggests that plugging occurred elsewhere in the SEDS. At this point, attempts were made to increase the flow rate of the gas through the SEDS. The increased flow would help to keep the particles from depositing along the tubing.

The configuration of the two vacuum pumps was modified to investigate the gas extraction. It was noticed that the suction from the SEDS sample probe was very low at atmospheric pressure. Tests of the sample extraction pump showed that it could not draw a representative sample from the low pressure CFFF flue duct. It was attempted to use the larger of the two pumps (the dilution pump) to pull samples into the probe as well as achieve sufficient dilution. However, even the larger pump could not extract a representative sample while driving the dilution of the SEDS. The smaller pump was reinstalled at the cyclone but plumbed so that its positive pressure side exhausted into the negative pressure of the large pump. This modification also failed to adequately extract a sample from the flue duct with appropriate dilution control. Since the Insitec calibration rig was operated at the same negative pressure as the flue duct, similar problems occurred while trying to do calibrations with Insitec. Figure 18 shows results from an Insitec/SEDS comparison. The figure shows that the SEDS has difficulty extracting a sample from the vacuum. Since the flow velocity in the SEDS is so low, most of the particles larger than about 0.7 microns extracted deposited along the tube walls.

Evidently the SEDS has difficulty in sampling from the flue duct at the CFFF, since the SEDS must pull a large volume of gas against the vacuum that is inside the duct. To overcome this problem, a pump with a larger volume capacity would be used to draw samples while another similar pump would provide all of the dilution. If the SEDS continues to plug, a two staged dilution would be used. This would create a high enough air velocity through the tubes to keep most of the larger particles from depositing along tube walls as well as keep the lines free from plugging. In this way, if each stage dilutes at

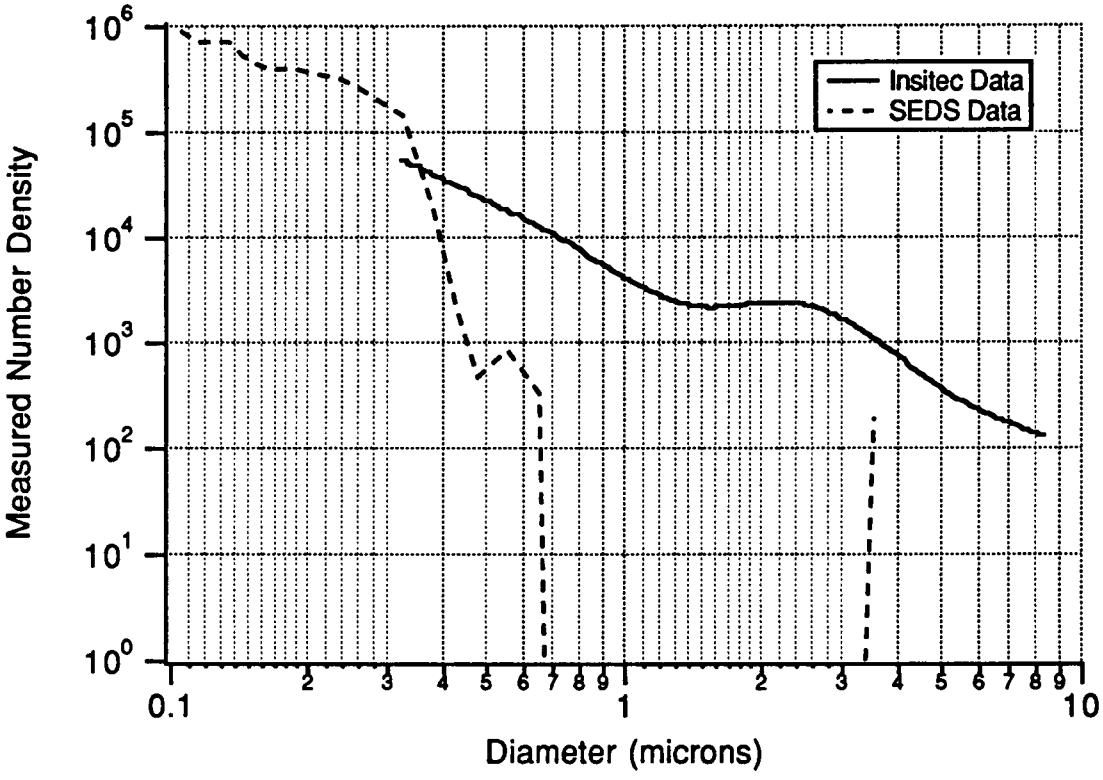


Figure 18. Calibration Comparison of SEDS and Insitec PCSV-UPF.

a 100:1 dilution ratio, 10,000:1 dilution is possible with orifices that are large enough so as not to become plugged. The sample of flue gas could also flow at higher rates and prevent depositing and plugging. The extra orifice, however, would add another uncertainty, as will be evident in the following sections.

In summary, the SEDS as configured did not operate correctly. Therefore, operating characteristics and overall uncertainty of the system could not be found. Since tests at the CFFF have been suspended, further tests to measure the overall uncertainty from the 5 stage cyclone and the Insitec calibration set up cannot be performed at this time.

Component Uncertainty

Nominal values for the measurements used in the uncertainty analysis will be taken as

t_o = 5 seconds,

R_{lo_o} = 0.2 cc per second for low flow rates,

R_{hi_o} = 2.0 cc per second for high flow rates,

α_o= 1

M_j = measured counts for the data set under consideration, and

Z_j = dilution ratio for the data set.

The influence coefficient for each variable is defined as

$$IC_{x_i} = \frac{\partial N}{\partial x_i}. \tag{27}$$

Multiplying the influence coefficient by the bias or random uncertainties yields a dimentionless measure for the uncertainties of the variables. In the following sections, the results of individual component uncertainties with the associated influence coefficients are presented.

Time Interval

As stated in chapter IV, the bias of the internal clock is $\pm 10^{-4}$ and the random error is $\pm 4.07 \times 10^{-7}$. This will result in

$$B_t = t \times 1 \times 10^{-4} \text{ sec}, \tag{28a}$$

$$S_t = t \times 4.07 \times 10^{-7} \text{ sec}. \tag{28b}$$

For t_o set to 5 seconds,

$$B_t = 5 \times 10^{-4} \text{ sec}, \qquad S_t = 2.04 \times 10^{-7} \text{ sec},$$

$$B_t IC_{t_{lo}} = 0.01 M_j, \qquad S_t IC_{t_{lo}} = 4.08 \times 10^{-5} M_j,$$

$$B_t IC_{t_{hi}} = 0.1 M_j, \qquad S_t IC_{t_{hi}} = 4.08 \times 10^{-6} M_j.$$

These errors contribute a negligible part to the overall uncertainty.

Sample Flow Rate

One of the PMS instruments (denoted 1 or *lo*) was used with a 0.2 cc per sec sample flow rate while the other (denoted 2 or *hi*) was used at its manufacturer's recommended sample flow rate of 2.0 cc per sec. The dynamic range of R is very limited; as the sample flow rate is reduced below the calibrated setting, more particles were placed in the smaller bin sizes. This is due to the fact that the inlet jet is positioned to focus the particles through the center of the laser for manufacturer's set flow rate only. When the flow rates are reduced, turbulent mixing between the sheath and sample air flows may occur in the sample volume and/or the particle stream may begin to deviate from the laser beam axis. Either of these conditions cause fewer particles to pass through the beam's center while more particles pass through the beam's edge where the radiation power is less, reducing the scattered radiation intensity for a given particle size. To correct this problem,

the ASASP-X with the low flow rate (0.2 cc/sec) had to be recalibrated after adjusting the inlet jet to refocus the particle stream.

Since the PMS instruments were to operate while drawing particles from a vacuum environment, measurements on the sample flow rate R variation were done at several different pressures while maintaining the same rotometer setting. Thirty measurements each were done at pressures ranging from 0 to 30 inches of water below atmospheric pressure for flow rates of 0.2 cc per second and 2.0 cc per second for the respective ASASP-X instrument. Table 3 shows the results.

As can be seen from the table, each of the mean flow rates lies well within 2 standard deviations of the other comparable mean values. Therefore, there is no correction for the flow rate when the spectrometers sample against a vacuum. With this in mind, the flow rates of the particle spectrometers will be taken to be the average of these means:

$$R_{lo} = 0.199 \text{ cc/sec},$$

$$R_{hi} = 2.107 \text{ cc/sec},$$

so the values of $B_{R_{hi}}$ and $B_{R_{lo}}$ are

$$B_{R_{hi}} = R_{hi} - R_{hi_o} = -0.107 \text{ cc/sec}, \tag{29a}$$

$$B_{R_{lo}} = R_{lo} - R_{lo_o} = 0.001 \text{ cc/sec}, \tag{29b}$$

and their random variations will be the standard deviations of the data sets:

$$S = \sqrt{\sum_{i=1}^{n} \left[\frac{(R_i - \langle R \rangle)^2}{n-1} \right]}, \tag{30}$$

$$S_{lo} = 3.68 \times 10^{-3} \text{ cc/sec},$$

$$S_{hi} = 4.14 \times 10^{-2} \text{ cc/sec}.$$

for the ASASP-X_{lo} and ASASP-X_{hi} respectively. These standard deviations will be used

Table 3. Results of Calibration Check for Sample Flow Meters.

Pressure of Vacuum (in. H_2O below atm)	Nominal Flow Rate cc/sec	Measured Average (30 measurements)	Standard Deviation
0	0.2	.01995	3.62×10^{-3}
10	0.2	0.1984	3.98×10^{-3}
20	0.2	0.1986	3.53×10^{-3}
30	0.2	0.1994	3.62×10^{-3}
0	2.0	2.1032	4.33×10^{-2}
30	2.0	2.1097	4.00×10^{-2}

to compute the maximum expected error limit for the flow rates when they are assumed to be steady. The influence coefficients are

$$B_{lo}IC_{R_{lo}} = 5M_j\,, \qquad S_{lo}IC_{R_{lo}} = 18.4M_j,$$

$$B_{hi}IC_{R_{hi}} = -5.35M_j\,, \qquad S_{hi}IC_{R_{hi}} = 2.07M_j.$$

Correction Factor

Since the flow rates were not steady, the value and uncertainties for α needs to be calculated. To find the value of α, 31 data sets were taken of room aerosol and fly ash while the spectrometers were sampling from both ambient pressure and the vacuum chamber. The rotometers were set at their nominal flow rates but were allowed to vary normally. Since no large difference could be seen between sampling from ambient pressure and sampling from a vacuum (any difference outside normal variations), all the data were weighted the same.

To attain statistical confidence, only results for particles of less than 0.45 microns in diameter were used here. Larger particles hardly reached the spectrometer that measured at a low 0.2 cc per sec sample flow rate. Low air flow and long tube length caused that some of the larger particles (greater than about 0.4 microns in diameter) deposit along the tube walls especially in lower density environments. Figure 19 shows results of both particle spectrometers sampling room air simultaneously. It can be seen that there is a good agreement in the low bins' sizes, but for particles larger than about 0.4 microns, the *dN/dD* values for the two instruments vary erratically because of the low number of total counts in the low flow rate instrument. For this reason, only the first 15 bins (diameters < 0.45 microns) were used to calculate the value of α, all of which had more than 1000 counts.

Since the α values for the first 15 bins are nearly identical, averaging over the statistically significant first 15 bins in accordance with equation 15 produces one α_i for the data set *i*

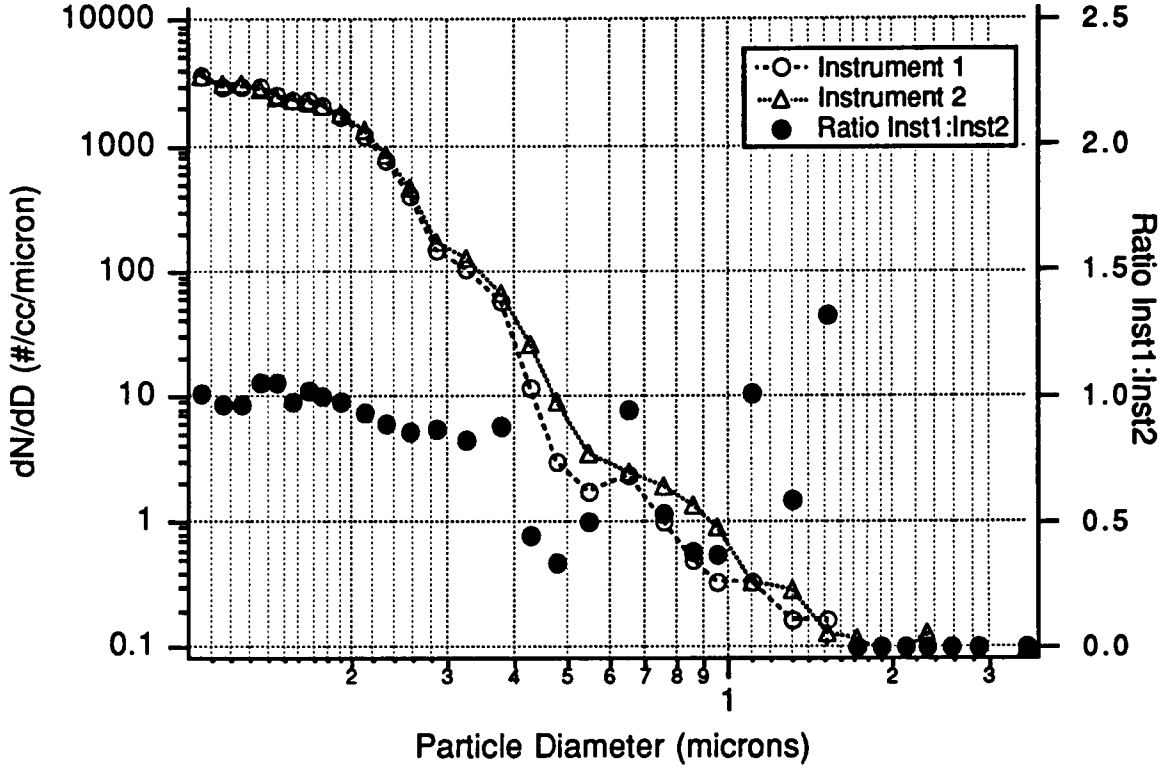


Figure 19. Divergence in Agreement Between Two Particle Spectrometers.

$$\alpha_i = \frac{1}{15}\sum_{j=1}^{15} \alpha_{ij}. \tag{31}$$

α_i is now a number that can be multiplied by N_{2_i} to correct for the variable flow rates over the data set i. Since the variation in flow rates was never the same, 31 different data sets were taken to achieve sufficient samples for statistical confidence. Using all 31 data sets, the bias and random error in α are calculated according to equations 17 and 18:

$$B_\alpha = \frac{1}{31}\left(\sum_{i=1}^{31} \alpha_i\right) - 1, \tag{32}$$

$$S_\alpha = \sqrt{\sum_{i=1}^{31}\left[\frac{(\alpha_i - \langle\alpha_i\rangle)^2}{30}\right]}. \tag{33}$$

These equations give a bias and standard deviation of

$$B_\alpha = 0.01613, \qquad S_\alpha = 0.1244,$$

$$B_\alpha IC_{\alpha_o} = 16.13M_j, \qquad S_\alpha IC_{\alpha_o} = 124.4M_j,$$

$$B_\alpha IC_{\alpha_i} = 1.613M_j, \qquad S_\alpha IC_{\alpha_i} = 12.44M_j.$$

It is apparent that the bias due to temporal variations in the sample flow rate is very small, less than 2% of the total flow, while the random error due to these fluctuations is much more significant, around 12% of the total flow. Coupled with the relatively high influence coefficient, we can see that the random fluctuations in flow through the rotometers cause an unacceptable error. A method for measuring or monitoring the flow rates as a function of time is necessary. A device such as an orifice or nozzle equipped with a pressure transducer or a vane type of flow meter is recommended.

Event Counting

The two instruments' accuracy of correctly sizing particles was verified with particles of known diameter. Data taken with PSL monodisperse particles show that there is a small spread away from the true spread in particle diameter, as seen in figures 20. Biases and random uncertainties were calculated according to equations 20 and 21. The data were taken with both instruments sampling the PSL particles from a vacuum of about 16 inches of water below atmospheric pressure. Samples were taken over a five minute period. Table 4 on pages 67 and 68 shows the data of figures 20 and the results of the statistical analysis are in table 5 on pages 69 and 70. Total biases and random errors are the average of the values for the individual measurements.

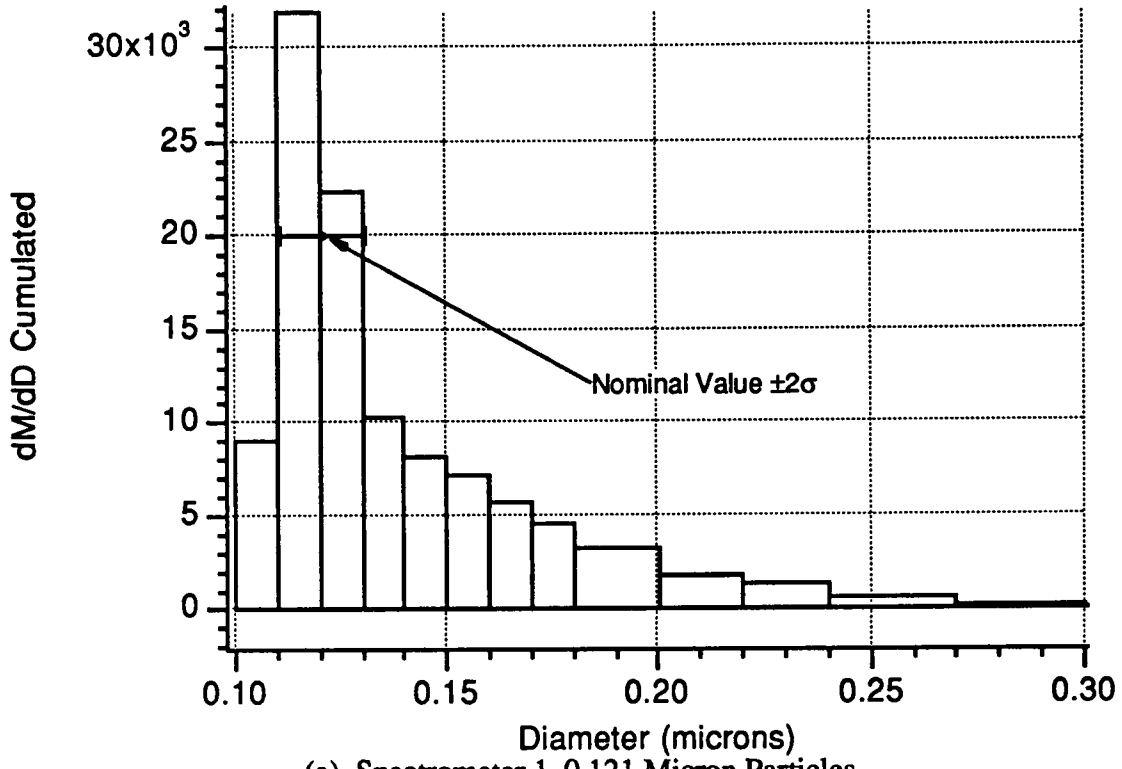
From the results of this analysis, the bias of the PMS instruments shifts the particle diameters to larger sizes by about one half percent of the actual particle size in the worst case. The random error for each instrument is about ten percent. The random error will make a significant contribution to the overall uncertainty limit due to the relatively large influence coefficient. These event counting errors will be taken as constant over the range of the instruments since the instrument calibration curves indicate similar size count variations. The biases and standard deviations along with the influence coefficients for each instrument are shown below.

$$B_{Mj_{lo}} = 0.0005M_j, \qquad S_{Mj_{lo}} = 0.099M_j,$$

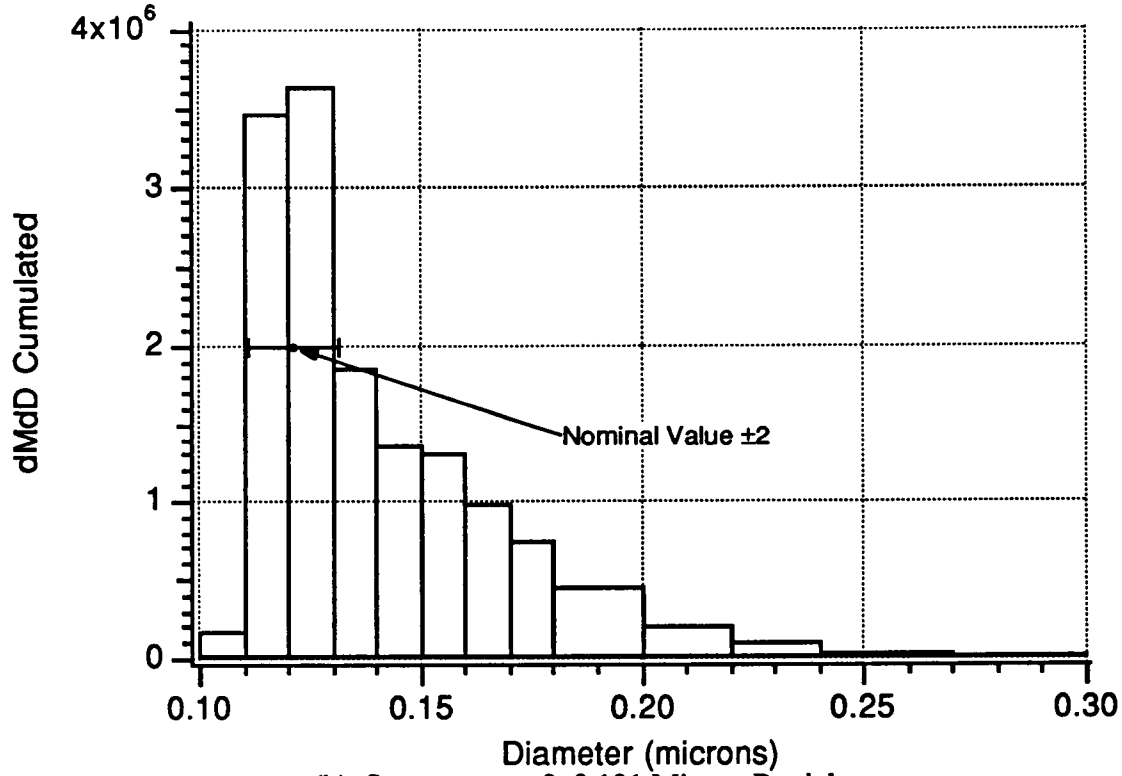
$$B_{Mj_{hi}} = 0.0004M_j, \qquad S_{Mj_{hi}} = 0.106M_j,$$

$$B_{Mj_{lo}}IC_{M_{lo}} = 0.05M_j, \qquad S_{Mj_{lo}}IC_{M_{lo}} = 9.9M_j,$$

$$B_{Mj_{hi}}IC_{M_{hi}} = 0.4M_j, \qquad S_{Mj_{hi}}IC_{M_{hi}} = 10.6M_j.$$

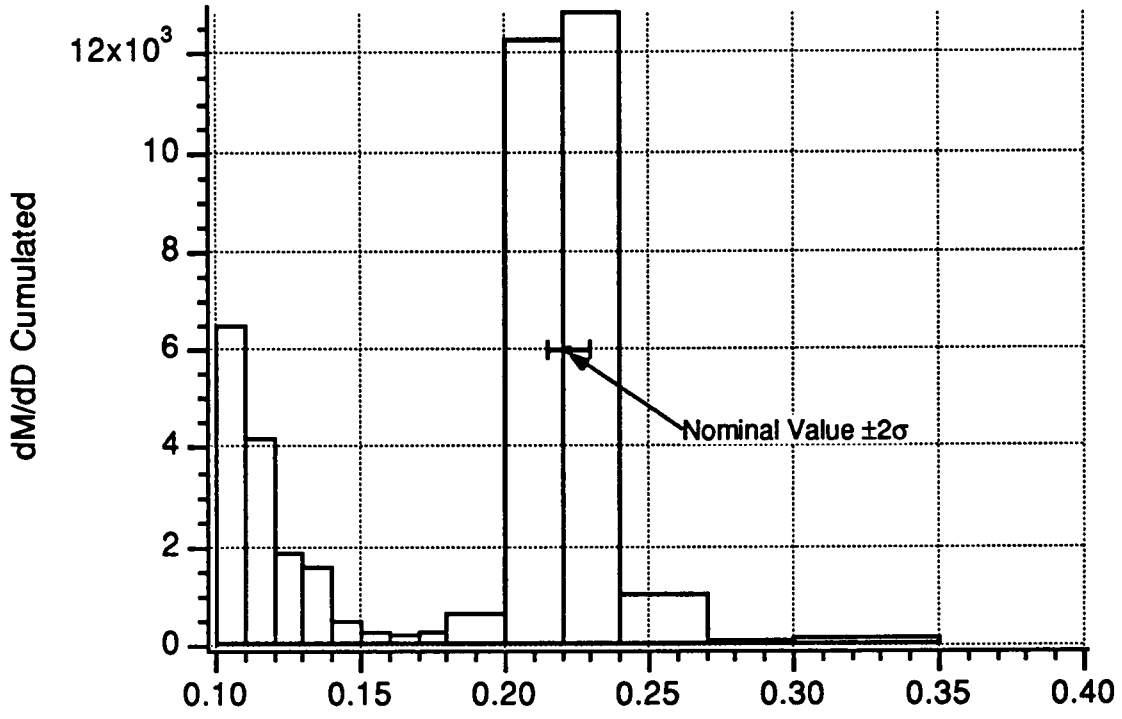


(a) Spectrometer 1, 0.121 Micron Particles.

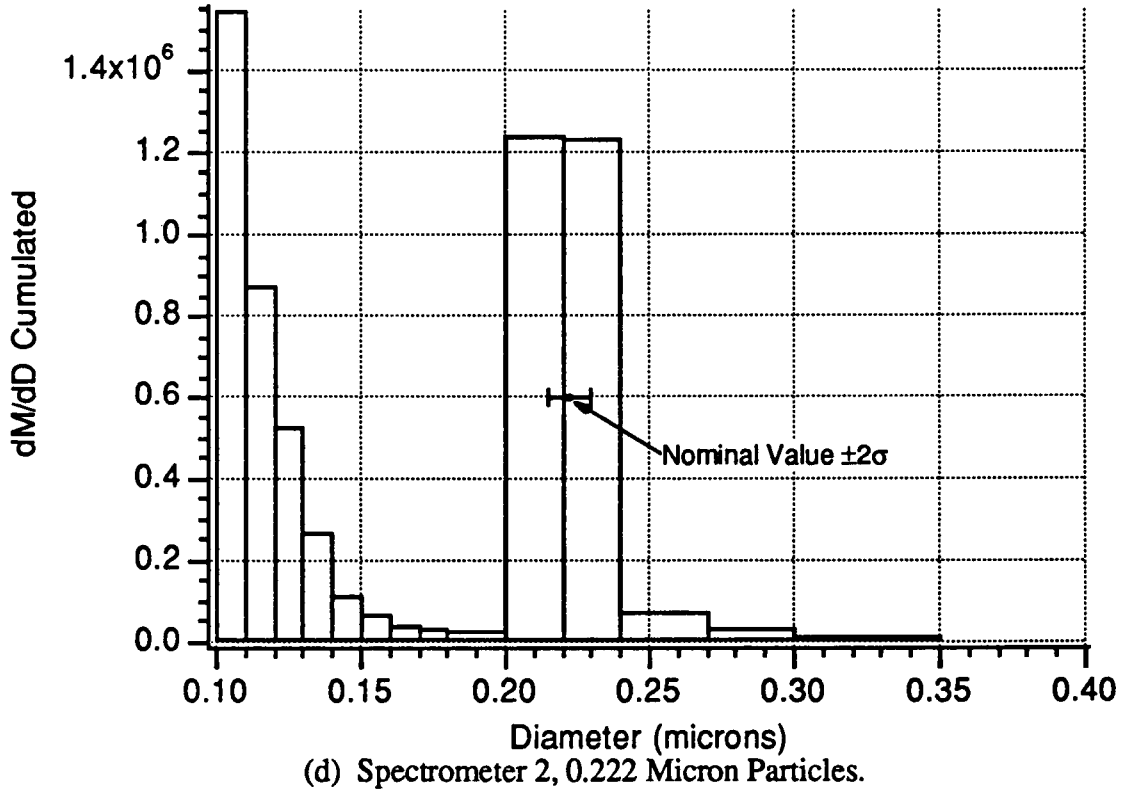


(b) Spectrometer 2, 0.121 Micron Particles

Figure 20. Measurements Made with Monodisperse Particles to Verify Accuracy in Response of ASASP-X.

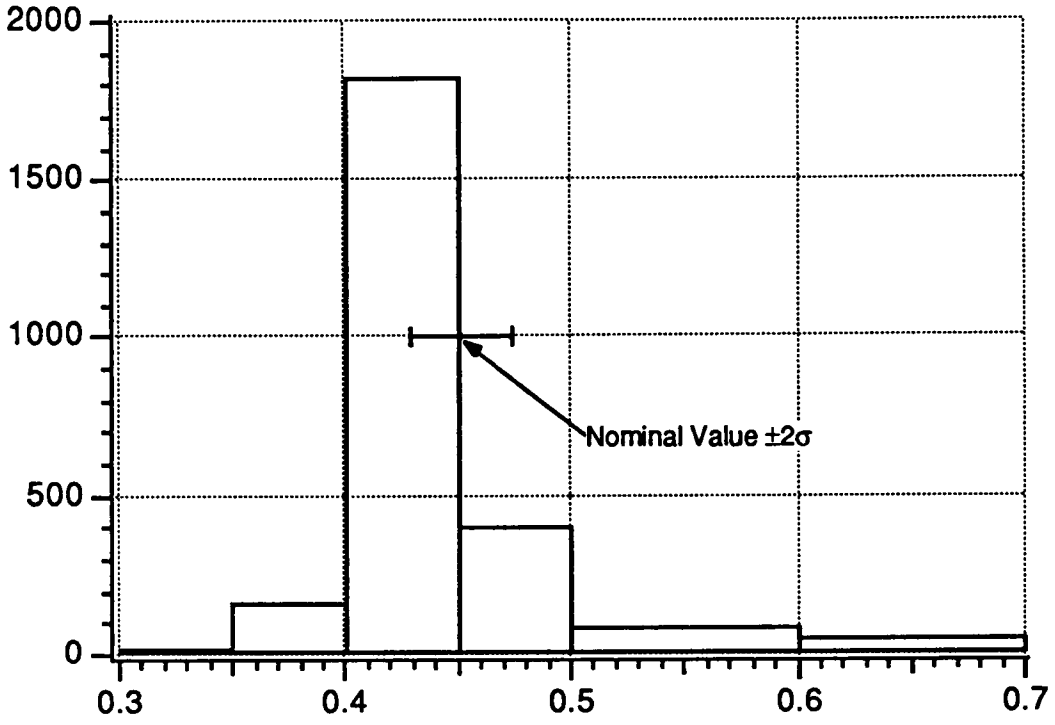


(c) Spectrometer 1, 0.222 Micron Particles

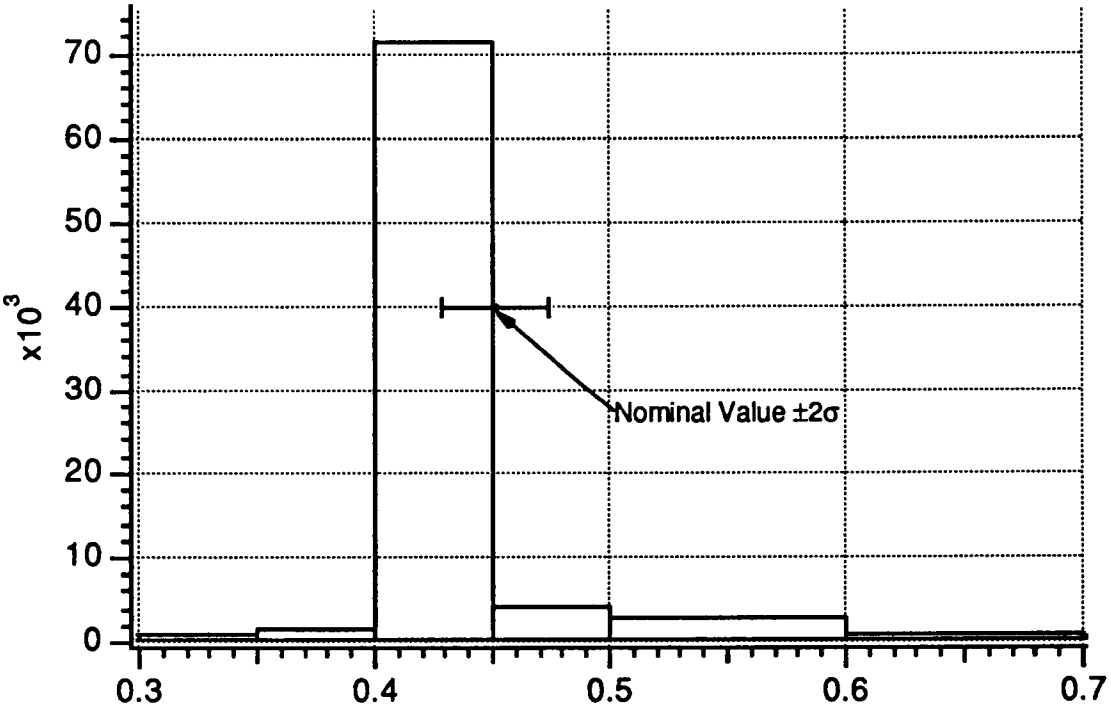


(d) Spectrometer 2, 0.222 Micron Particles.

Figure 20 (Continued).

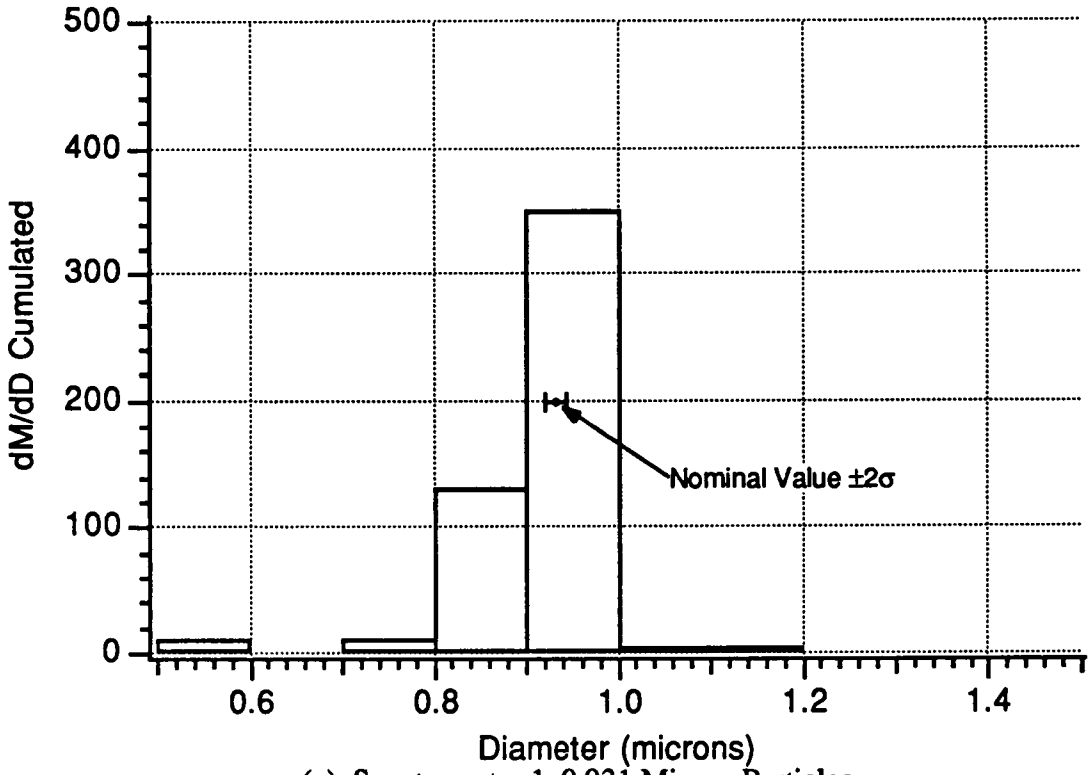


(e) Spectrometer 1, 0.451 Micron Particles.

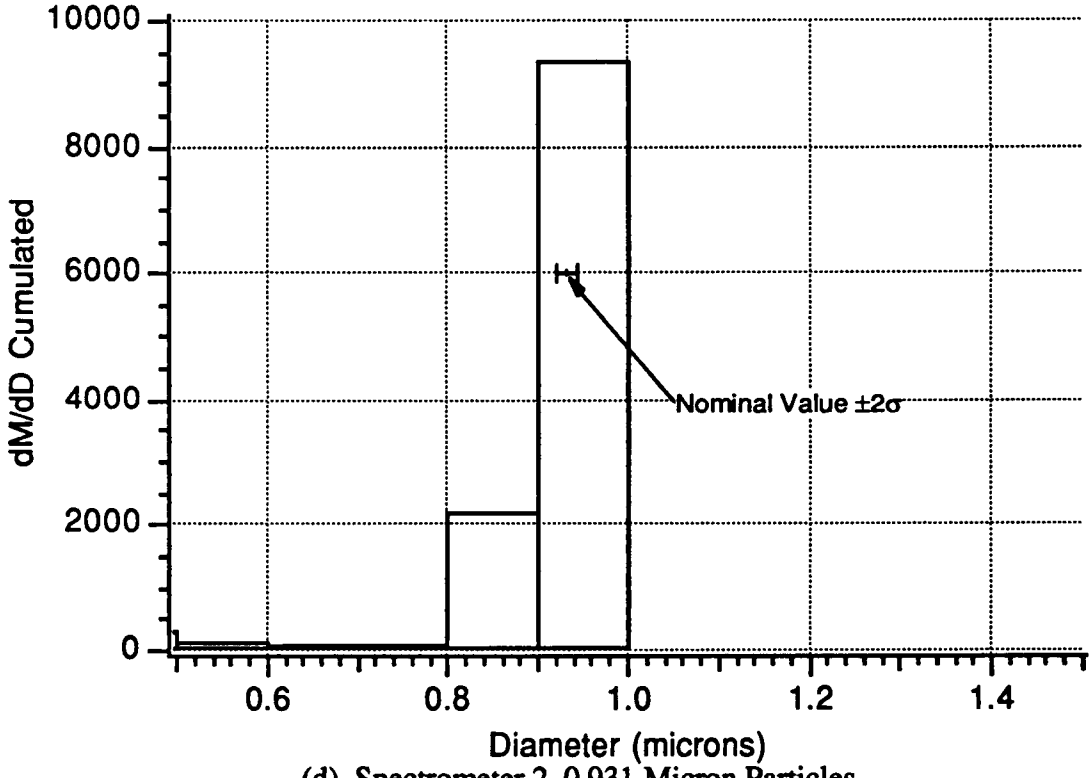


(f) Spectrometer 2, 0.451 Micron Particles.

Figure 20 (Continued).



(c) Spectrometer 1, 0.931 Micron Particles.



(d) Spectrometer 2, 0.931 Micron Particles.

Figure 20 (Continued).

Table 4. Results of Measurements to find *M* and its Uncertainties.

Mean Bin Diameter Microns	Instrument 1 Counts / Micron	Instrument 2 Counts / Micron
Particle Diameter 0.121 Microns		
0.105	9000	171600
0.115	31900	3461000
0.125	22400	3635600
0.135	10400	1860700
0.145	8100	1358600
0.155	7200	1299300
0.165	5700	986000
Particle Diameter 0.222 Microns		
0.165	200	42900
0.175	300	30300
0.190	650	26750
0.210	12300	1236150
0.230	12850	1231450
0.255	1033.3	75933.3
0.285	100	33633.3
0.325	160	13820
0.375	0	1820

Table 4. (Continued)

Mean Bin Diameter Microns	Instrument 1 Counts / Micron	Instrument 2 Counts / Micron
Particle Diameter 0.451 Microns		
0.285	0	900
0.325	20	880
0.375	160	1720
0.425	1820	71460
0.475	400	4260
0.550	90	2980
0.650	50	900
0.750	0	680
0.850	0	480
Particle Diameter 0.931 Microns		
0.55	10	150
0.65	0	70
0.75	10	100
0.85	130	2210
0.95	350	9350
1.10	5	20
1.30	0	0
1.50	0	10
1.70	0	15

Table 5. Summary of Measurements to find *M* and its Uncertainties.

Parameter	Instrument 1	Instrument 2
0.121 Micron Diameter PSL Spheres		
Total Counts per Micron (dM/dD)	94730	13272800
Averaged Measured Diameter (Microns)	0.1272	0.1268
Bias Uncertainty (Average - PSL Diameter)	0.00619	0.00578
Fractional Bias Uncertainty (Bias / PSL Diameter)	0.0511	0.0478
Random Uncertainty (Standard Deviation)	0.01663	0.01653
Fractional Random Uncertainty (Random / PSL Diameter)	0.137	0.137
0.222 Micron Diameter PSL Spheres		
Total Counts per Micron (dM/dD)	27593.3	2692756.7
Averaged Measured Diameter (Microns)	0.2208	0.2207
Bias Uncertainty (Average - PSL Diameter)	-0.0012	-0.0013
Fractional Bias Uncertainty (Bias / PSL Diameter)	-0.00541	-0.00586
Random Uncertainty (Standard Deviation)	0.0168	0.0182
Fractional Random Uncertainty (Random / PSL Diameter)	0.0757	0.0820

Table 5. (Continued).

Parameter	Instrument 1	Instrument 2
0.451 Micron Diameter PSL Spheres		
Total Counts per Micron (dM/dD)	2540	84260
Averaged Measured Diameter (Microns)	0.4378	0.4359
Bias Uncertainty (Average - PSL Diameter)	-0.0132	-0.01516
Fractional Bias Uncertainty (Bias / PSL Diameter)	0.0293	0.0336
Random Uncertainty (Standard Deviation)	0.0464	0.0579
Fractional Random Uncertainty (Random / PSL Diameter)	0.103	0.128
0.931 Micron Diameter PSL Spheres		
Total Counts per Micron (dM/dD)	505	11925
Averaged Measured Diameter (Microns)	0.9139	0.925
Bias Uncertainty (Average - PSL Diameter)	-0.0171	-0.0064
Fractional Bias Uncertainty (Bias / PSL Diameter)	-0.0184	-0.0069
Random Uncertainty (Standard Deviation)	0.0739	0.0713
Fractional Random Uncertainty (Random / PSL Diameter)	0.0794	0.0766

Dilution Ratio

The theoretical uncertainties of the dilution ratios (Z_j) are calculated from the various uncertainties in all parameters. Table 6 lists the parameters, their nominal values, the influence coefficients, and the error contribution from each parameter. By inserting these results into equations 23, the following values for the bias B and random error S in the theoretical dilution factor Z were found:

$$B_Z = 0.0242, \qquad S_Z = 0.181,$$

$$B_Z IC_{Z_{lo}} = 0.0242 M_j, \qquad S_Z IC_{Z_{lo}} = 0.181 M_j,$$

$$B_Z IC_{Z_{hi}} = 2.42 \times 10^{-4} M_j, \qquad S_Z IC_{Z_{hi}} = 1.81 \times 10^{-3} M_j.$$

Total Theoretical Uncertainty Limit

To calculate the particle number density in the flue stream, equation 3 modified with the correction factor α is used:

$$N_j = \frac{M_j Z_j}{\alpha R t}. \tag{34}$$

By using equation 34 in equation 10, the derivative with respect to α is included and the overall bias and random error limits are

$$B = \sqrt{\left(\frac{Z}{\alpha R t} B_M\right)^2 + \left(\frac{M}{\alpha R t} B_Z\right)^2 + \left(\frac{MZ}{\alpha^2 R t} B_R\right)^2 + \left(\frac{MZ}{\alpha R^2 t} B_R\right)^2 + \left(\frac{MZ}{\alpha R t^2} B_t\right)^2}, \tag{35a}$$

$$S = \sqrt{\left(\frac{Z}{\alpha R t} S_M\right)^2 + \left(\frac{M}{\alpha R t} S_Z\right)^2 + \left(\frac{MZ}{\alpha^2 R t} S_R\right)^2 + \left(\frac{MZ}{\alpha R^2 t} S_R\right)^2 + \left(\frac{MZ}{\alpha R t^2} S_t\right)^2}. \tag{35b}$$

Table 6. Results of Measurements to find Z and its Uncertainties.

Variable	Definition	Nominal Value	Influence Coefficient	Random Error	Bias Error
K_L	Large Orifice Calibration Constant	169.41	0.0328	4.4 § (2.6%)	0.312§
K_S	Small Orifice Calibration Constant	70.925	-0.0911	0.39 § (0.56%)	-0.231§
P_L	Pressure, High Pressure Side, Large Orifice (inches of water)	-11	0.115	0.22 (2%)*	--
P_S	Pressure, High Pressure Side, Small Orifice (inches of water)	-6	-0.113	0.12 (2%)*	--
TL	Temp of Gas through Large Orifice (F)	77	-0.00602	3.96* (5.14%)	--
T_S	Temp of Gas through Small Orifice (F)	176	0.00508	3.96* (2.25%)	--
mw_{wet}	Wet Molecular Weight of Carrier Gas	31	0.000112	0.3† (0.97%)	--
f	Mass Fraction of Water is Sample Gas	0.16	-0.0252	0.01‡ (1%)	--
ΔP_L	Pressure Drop across Large Orifice (inches of water)	1.1	0.439	0.022 (2%)*	--
ΔP_S	Pressure Drop across Small Orifice (inches of water)	3.6	-0.208	0.066 (2%)*	--
b_L	Curve Fitting Constant of Large Orifice	0.3579	0.121	0.16§ (44%)	0.2405§
b_S	Curve Fitting Constant of Small Orifice	0.6096	-1.572	0.0141§ (2.3%)	0.0006§
BP	Barometric Pressure (inches of Mercury)	29	0.000141	0.029 (0.1%)	--

§ See Appendix 2 for detailed calculations.
* Manufacturer's Specifications.
† From Repeated Observations.
‡ EPA method 4 [19].

Table 7 lists the values of all the variables in equations 35. By using these values, calculation of the limits on bias random error and uncertainty as of equation 7 yields

$$B_{lo} = 1.76\%, \qquad B_{hi} = 1.75\%,$$

$$S_{lo} = 16.0\%, \qquad S_{hi} = 16.5\%,$$

$$U_{lo} = 32.1\%, \qquad U_{hi} = 33.0\%.$$

The uncertainty calculation reveals an uncertainty limit of more than 30% for each of the spectrometers. Most of this error comes from the inability to monitor the variations in the flow rate. Without these errors ($B_\alpha = S_\alpha = 0$), the uncertainty limits decrease to

$$B_{lo} = 0.44\%, \qquad B_{hi} = 0.50\%,$$

$$S_{lo} = 10.8\%, \qquad S_{hi} = 10.1\%,$$

$$U_{lo} = 21.6\%, \qquad U_{hi} = 21.3\%.$$

Table 7. Final Uncertainty Analysis for SEDS.

Variable	Nominal Value	Influence Coefficient	Bias Error	Random Error
Low Sample Flow Rate System				
M_j	M_i	1000	$0.005M_j$	$0.099M_i$
Z	1000	M_i	0.0242	0.181
α	1	$1000M_i$	0.01613	0.1244
R	0.2	$5000M_i$	0.001	3.68×10^{-3}
t	5	$200M_j$	5×10^{-4}	2.04×10^{-6}
N	$1000M_i$	--	$26.2M_i$	$149M_i$
High Sample Flow Rate System				
M_j	M_i	100	$0.004M_i$	$0.106M_i$
Z	1000	$0.01M_i$	0.0242	0.181
α	1	$100M_i$	0.01613	0.1244
R	2	$50M_i$	-0.107	0.0414
t	5	$20M_i$	5×10^{-4}	2.04×10^{-6}
N	$100M_i$	--	$5.94M_i$	$14.9M_i$

CHAPTER VI

Conclusions and Recommendations

There is a continued need in the environmental community for an on-line, near real time particulate monitor to evaluate accurately the collection efficiencies of baghouse and electrostatic precipitators and to assess the effect that changes in plant operating conditions or fuel chemistry have on the efficiencies. The Sample Extraction / Dilution System promises to offer the necessary capability if the problems with the system are resolved. While taking measurements in conjunction with the 5 stage cyclone, the SEDS did not work properly due to plugging in the lines of the system or saturating the particle measuring device used in the SEDS.

Because the SEDS did not perform properly it was not possible to determine the overall operating characteristics or the uncertainties of the system. Estimates of the uncertainty due to component uncertainties were provided. Results showed the total uncertainty limit to be over 30%. To reduce this error it is recommended to better control the sample flow rates in the PMS instruments and/or better monitor flow rates for the instruments. If the sample flow rate could be kept steady with time or if it could be monitored and changes recorded with time, then the problem with variable flow rate errors would be eliminated. The uncertainty of the rotometer would be replaced with that of a new flow meter (such as an orifice type meter) and the correction factor α would not be required. In this case it is estimated that the overall uncertainty limit would reduce to about 20%.

Future work needs to be done on the SEDS. As a result of this study, it is recommended that a larger pump be used to extract the samples of particle laden gas from

the CFFF flow train. This would enable more representative sampling from the duct and alleviate plugging within the SEDS. Also, a two staged dilution system for the SEDS should be developed to eliminate plugging. With two stages of dilution, each of 100 to 1, dilution ratios of 10,000 to 1 are possible. However, additional measurement uncertainties are introduced with a second stage. The effect on the overall uncertainty will be small since the influence coefficient of the dilution variable Z is small. It is estimated that an increase of 100 times in the error of Z will increase the overall uncertainty by about 0.1%, based on the theoretical prediction. If a two staged dilution is used, a study will need to be made of the effect that the extra dilution chamber has on the response time of the SEDS.

A third recommendation is to do a quantitative study about how the activity of the PMS instruments affects the reported size distribution. The instrument's manufacturer suggests an algorithm to correct for the masking effect of the smaller bin sizes. If the instrument's response were well known at the high activity rates, it would be possible to increase the total number of particles detectable in an accurate way by weighting the number counts in the proper way.

LIST OF REFERENCES

LIST OF REFERENCES

[1] Newton, G. H., Schieber, C., Socha, R. G., and Kramlich, J. C., "Mechanisms Governing Fine Particulate Emission from Coal Flames", DOE Contract Report DOE/PC/79743-TB (DE 92014840) Energy and Environment Research Corporation, Irvine, CA April 1990.

[2] Allen, Terrance, *Particle Size Measurement, 4th ed.*, Chapman and Hall, New York, 1990.

[3] McElroy, M., Carr, R., Ensor, D., and Markowsky, G., "Size Distribution of Fine Particles from Coal Combustion", *Science*, Vol. 215, No. 4528, 1982.

[4] Andol, J., and Lindner, J. S., "CFFF LMF5-G Diagnostic Measurements--Two Color Laser Transmissometer", Mississippi State University, DIAL Data Report, Vol. 12, No. 6, Dec. 1992.

[5] Holve, D. J. and Bonnin, M. P., "*In Situ* Measurements of Particulate Emissions from MHD Combustion Processes", First Semi-Annual Report, DOE Grant # De - FG03 - 91ER81124, Nov. 1992.

[6] Ragland, J. W., McCain, J. D., and Smith, W. B., "Design, Construct, and Test a Field Usable Prototype System for Sizing Particles Smaller than 0.5 Micron Diameter", Draft EPA Contract Report SORI - EAS - 78 - 234, Southern Research Institute, April 1978.

[7] Active Scattering Aerosol Spectrometer Probe, PMS Model ASASP-X Operating and Servicing Manual, Particle Measuring Systems, Inc., Boulder, CO Oct. 1991.

[8] Waddell, V. A., "Mie Analysis of Geometries for Phase Angle Particle Sizing Interferometry", Master of Science Thesis, The University of Tennessee, Knoxville, Tennessee, August 1986.

[9] Hodkinson, J. D. and Greenleaves, I., "Computations of Light Scattering and Extinction by Spheres According to Diffraction and Geometrical Optics, and some Comparisons with the Mie Theory", *Journal of the Optical Society of America*, Vol. 53, 577 - 588, 1953.

[10] Van de Hulst, H. C. *Light Scattering by Small Particles*, Wiley, New York, 1957.

[11] Born, M. and Wolf, E., *Principles of Optics: Electromagnetic Theory of Propagation, Interference, and Diffraction of Light*, Pergaman Press, New York, 1975.

[12] Pinnick, R. G. and Auvermann, H. J., "Response Characteristics of Knollenberg Light-Scattering Aerosol Counters", *Journal of Aerosol Science*, Vol. 10, 55-74, 1979.

[13] Personal Communication, Requested Mie Scattering Calculations for the ASASP-X Particle Measuring Systems, 1992

[14] Personal Communication, Particle Measuring Systems, 1993.

[15] Abernathy, B., "Fluid Flow Measurement Uncertainty", Draft Revision of ISO/DIS 5168 for International Organization for Standardization Committee, ISO TC305C9 , May 1987.

[16] Smart Probe Version 3.2 Operating and Service Manual, Particle Measuring Systems, Inc., Boulder, CO Oct. 1991.

[17] Digi-Key Corporation Catalog, Thief River, MN, July/August 1993.

[18] Baumeister, T., Editor, *Mark's Standard Handbook for Mechanical Engineers, Eighth Ed.*, McGraw-Hill Inc., 3-60 - 3-64, NY 1978.

[19] Smith, Walter G., Compiler, "EPA Stationary Source Sampling Methods Notebook (NSP and NSHAPS Methods)", McIlvaine Co., Northbrook, IL 1984.

APPENDICES

APPENDIX A

Commercially Available Particulate Sizing Instruments Considered for the SEDS

The following list is a description of some of the instrumentation available for particle sizing and the limitations of these instruments [1].

Bausch and Lomb

The Bausch and Lomb dust counter uses near forward light scattering and captures the scattered light through an angle from 24° to 40°. The light is reflected from a parabolic mirror to a photomultiplier tube. The instrument has a built in calibration system and operates in size ranges from 0.3 to 10 microns. It also has a built in dilution system, but still only allows for measuring concentrations of up to 10^6 particles per cubic foot (about 35 per cm^3) which is not sufficient for the CFFF.

Climet Series 7000

The CI 7500 operates with a He-Ne laser. The sizing is at 0.1, 0.2, 0.3, 0.4, and 0.5 microns. This size range does not extend to large enough particles. Other CI 7000 series instruments, although they offer larger size ranges, have poorer size resolution that are similar to the 5 stage cyclone.

Dynac

The Dynac M201C measures airborne particulate of size ranges from 0.15 to 5 microns, but only has the capability to count to 770 particles per cm^3. This number is far below the requirements to measure the high CFFF particle concentrations.

Gardner

The Gardner small particle detector uses a condensation nuclei concept. Under suitable conditions, water vapor condenses on the particles, allowing for measurements of particles with diameters of down to 1 nanometer. However, "suitable conditions" may not exist at the CFFF where particle sampling needs to take place.

Techecology

The Techecology Model 200 is inappropriate due to poor size resolution (0.5, 1.0, 2.0, 5.0, 10.0, >10.0 microns) and due to limited concentration capability (up to 350 particles per cm^3).

APPENDIX B

Calculation of Orifice Calibration Parameters *K* and *b* and Their Respective Uncertainties

The equation for the flow of gas through an orifice is

$$Q = K\sqrt{\frac{Pmw}{T_R}}(\Delta P)^b, \tag{B1}$$

where

Q = mass flow of gas through the orifice,

P = static pressure on high pressure side of the orifice,

mw = molecular weight of the gas

T_R = temperature of gas (Rankine scale),

ΔP = pressure drop across the orifice,

K = orifice calibration constant, and

b = parameter that causes the curve to best fit experimental data.

Measurements were made on two orifices, the large dilution air orifice and the small sample air orifice. The data are summarized in table B1.

By rearranging equation B1, we write the expression as

$$Q\sqrt{\frac{T_R}{Pmw}} = K(\Delta P)^b. \tag{B2}$$

The left hand side of equation B2 is assigned to the variable Q'. The same adjustments were made for T and P as were made in equation 19b, that is

Table B1. Data Points for Calibration Constant Calculation.

	Q gm / min.	T_F Fahrenheit	P inches of water	ΔP inches of water
Large Orifice				
	184	98	-35.5	0.85
	205	100	-46.5	1.05
	223	99	11.5	1.23
Small Orifice				
	54.2	77	0.41	0.45
	75.2	77	0.75	0.76
	103.2	77	1.28	1.28

$$T_R \Rightarrow T_F + 459.67, P \Rightarrow BP + P/13.6,$$

yielding

$$Q' = Q\sqrt{\frac{T_F + 459.67}{mw\left(BP + \frac{P}{13.6}\right)}}, \tag{B3}$$

so that

$$Q' = K(\Delta P)^b. \tag{B4}$$

Using a chi-squared minimization method, a curve was fit to the data points in table B1 that calculated the best value for K and b as well as their standard deviations. These values are:

$K_L = 169.41,$ $K_S = 70.925,$

$S_{KL} = 4.4,$ $S_{Ks} = 0.39,$

$b_L = 0.3597,$ $b_S = 0.6096,$

$S_{bL} = 0.16,$ $S_{bs} = 0.0141.$

To find the bias in K, equation B4 is rearranged and solved for K

$$K = \frac{Q'}{(\Delta P)^b}. \tag{B5}$$

By assuming constant b at its fitted value, values for K are calculated using the various values of Q' and ΔP. The bias in K will be the difference of the average of these calculation and its fitted value,

$$K_{calc} = \frac{1}{3}\sum_{i=1}^{3} K_i, \tag{B6}$$

$$B_K = K_{fit} - K_{calc}. \tag{B7}$$

The bias of b is estimated in a similar way. Rearranging equation B4 and solving for b, the new equation is

$$b = \frac{\ln(Q') - \ln(K)}{\ln(\Delta P)}. \tag{B8}$$

K is held constant at its fitted value and b's are calculated using values for Q' and ΔP. The bias is also the difference of the fit b and the average of these calculated values:

$$b_{calc} = \frac{1}{3}\sum_{i=1}^{3} b_i, \tag{B9}$$

$$B_b = b_{fit} - b_{calc}. \tag{B10}$$

Table B2 lists the results of this analysis. The biases are

B_{KL} = 0.312, B_{Ks} = -0.231,

B_{bL} = 0.241, B_{bs} = 0.0006.

Table B2. Results of Uncertainty Analysis for Orifice Calibration Constants.

Large Orifice	Q'	ΔP	K_{fit}	K_{calc}	b_{fit}	b_{calc}
Large Orifice						
	157.07	0.85	169.41	166.47	0.3579	0.4651
	178.39	1.05	169.41	175.30	0.3579	1.0586
	179.19	1.23	169.41	166.39	0.3579	0.2701
Small Orifice						
	43.27	0.45	70.952	70.411	0.6096	0.6192
	60.02	0.76	70.952	70.945	0.6096	0.6100
	82.31	1.28	70.952	70.806	0.6096	0.6013

VITA

Jack Leland Parker was born on October 23, 1964, in Salt Lake City, Utah. He graduated from Los Alamos High School in Los Alamos, New Mexico in 1983. After serving a 2 year mission in Brazil for the Church of Jesus Christ of Latter-day Saints from 1984 - 1986, he entered Brigham Young University in Provo, Utah and graduated with a Bachelor of Science Degree in Physics in April of 1991. In the fall of 1991, he began graduate studies in physics at the University of Tennessee Space Institute in Tullahoma, Tennessee.

In July of 1992, he married the former Collette Wilson of Albuquerque, New Mexico. They have one daughter, Samantha Leigh, born in September of 1993.